A Stochastic-Statistical Residential Burglary Model with Finite Size Effects

Chuntian Wang, Yuan Zhang, Andrea L. Bertozzi and Martin B. Short

Abstract Transience of spatio-temporal clusters of residential burglary is well documented in empirical observations, and could be due to *finite size effects* anecdotally. However a theoretical understanding has been lacking. The existing agent-based statistical models of criminal behavior for residential burglary assume deterministic time steps for arrivals of events. To incorporate random arrivals, this article introduces a Poisson clock into the model of residential burglaries, which could set time increments as independently exponentially distributed random variables. We apply the Poisson clock into the seminal deterministic-time-step model in [M. B. Short, M. R. D'Orsogna, V. B. Pasour, G. E. Tita, P. J. Brantingham, A. L. Bertozzi, and L. B. Chayes, *Math. Models Methods Appl. Sci.*, 18, (2008), pp. 1249-1267]. Introduction of the Poisson clock not only produces similar simulation output, but also brings in theoretically the mathematical framework of the Markov pure jump processes, e.g., a martingale approach. The martingale formula leads to a continuum equation that coincides with a well-known mean-field continuum limit. Moreover, the martingale formulation together with statistics quantifying the relevant pattern formation leads to a theoretical explanation of the *finite size effects*. Our conjecture is supported by numerical simulations.

Chuntian Wang
University of California, Los Angeles, Los Angeles, USA,
e-mail: cwang@math.ucla.edu.

Yuan Zhang
Peking University, Beijing, P. R. China,
e-mail: zhangyuan@math.pku.edu.cn.

Andrea L. Bertozzi
University of California, Los Angeles, Los Angeles, USA,
e-mail: bertozzi@ucla.edu.

Martin B. Short
Georgia Institute of Technology, Atlanta, GA, USA,
e-mail: mbshort@math.gatech.edu.

1 Introduction

Crime is an unfortunate aspect of modern life that takes place in every major urban area. In the past ten years quantitative scientists have been working in the burgeoning area of crime modeling and prediction (e.g. [3, 4, 28, 29, 46, 48, 52, 55, 57, 61, 62, 63, 67, 71, 72, 73, 74, 75, 76, 77, 81, 83, 84]). Crime is not uniformly distributed in space and time but rather exhibit spatio-temporal aggregates of criminal occurrences that are referred to as crime "hotspots". The first model to quantify such patterns is an agent-based human environment interaction model assuming deterministic time steps (DTS Model [76]). Follow-up works show that such simple models can exhibit both crime displacement and crime suppression in the presence of police activity [74, 73]. In all these works *finite size effects* were observed: discrete simulations show both transient and stationary hotspots, while continuum simulations show only stationary hotspots. As criminal number decreases, discrete simulations exhibit more transience, and crime population is finite size actually in real life. Therefore, a deeper understanding of these effects is relevant to real crime statistics [61, 28]. Moreover, the DTS Model [76] assumes deterministic-time arrivals of events, however, criminals act randomly in reality. Models setting random arrivals are called for.

In this work, with the application of a Poisson clock to the DTS Model [76], the time increments are made into independently exponentially distributed random variables. Introduction of the Poisson clock not only exhibits similar simulation output, but also brings in theoretically the mathematical framework of Markov pure jump processes and interacting particle systems ([14, 47, 49, 50, 51]).

The Poisson clock is the basic element to build a Poisson point process, which is particularly suitable to model random arrivals. Poisson point process is one of the most studied and used point processes in probability and in more applied disciplines such as biology, economics, and physics (see e.g. [2, 5, 13, 18, 27, 65]). Normally independent Poisson clocks are assumed for each agent. Nevertheless assuming a uniform Poisson clock is helpful here, as it is more computationally efficient. Moreover, a martingale approach for the Markov pure jump processes is applicable. The martingale formulation is a useful tool to analyze both statistical and stochastic aspects of the model, and expresses the model as the summation of two components: a predictable or deterministic component and a stochastic or unpredictable component. As far as we know this is the first time that the stochastic component of the model is mathematically demonstrated.

The deterministic component serves as a continuum model that is parallel to the discrete one. The continuum Poisson-clock model turns out to be the same as the continuum DTS Model [76]. More importantly, the martingale formulation leads to a theory for the *finite size effects* thanks to the demonstration of the stochastic component. To quantify pattern formation for the *finite size effects*, we construct statistics to measure the degree of hotspot transience. These statics could be applied to general pattern formation problems. We find that a scaling property of the stochastic component with varying criminal population is the key to the theory of *finite size effects*. As the total criminal population decreases, the stochastic compo-

nent increases while the deterministic component remains fixed. We conjecture that this is the mechanism behind the *finite size effects*. Our conjecture is supported by numerical simulations. The study is also in line with the scaling of initial data of hydrodynamic limit approximations for interacting particle systems ([24]). In general the initial total particle number is assumed to increase as the lattice grid decreases so that the initial density remains fixed. This has been treated so far as merely a technicality and is rarely explored analytically nor computationally. However in the applications the details are important because the real world is of finite size.

The article is organized as follows. In Section 2, the discrete Poisson-clock model is introduced (Section 2.1) and the martingale formulation is established (Section 2.2). Based on the formulation a continuum model is derived (Section 2.3). The finite size effects are analyzed in Section 3. Statistics are constructed to quantitatively measure the degree of hotspot transience (Section 3.1). A theory of the *finite size effects* is explored (Section 3.2). Section 4 is about future works. The Appendix shows the derivation of the martingale formulation.

2 Poisson-clock model

2.1 Discrete model

The discrete Poisson-clock model is the same as the DTS Model [76], with the only exception of introduction of the Poisson clock.

2.1.1 Introduction of the Poisson clock

The discrete model consists of two components — the stationary burglary sites and a collection of burglar agents jumping from site to site. We assume the domain to be $\mathscr{D} := [0,L] \times [0,L]$ with the periodic boundary conditions[1]. The lattice grid over $\mathscr{D}$ has spacing $\ell = 1/N$, $N \in \mathbb{N}$. The grid points are denoted as $\mathbf{s} = (\mathbf{s}_1, \mathbf{s}_2)$, $\mathbf{s}_1 = \ell, 2\ell, \cdots, L$, $\mathbf{s}_2 = \ell, 2\ell, \cdots, L$. The collection of all the grid points is denoted as $\mathscr{S}^\ell$. Attached to each $\mathbf{s} \in \mathscr{S}^\ell$ is a pair $(n^\ell_{\mathbf{s}}(t), A^\ell_{\mathbf{s}}(t))$ representing the number of criminal agents and attractiveness at site $\mathbf{s}$ at time t. The attractiveness stands for the burglar's beliefs about the vulnerability and value of the target site. We also assume that $A^\ell_{\mathbf{s}}(t)$ consists of two parts, a dynamic term and a static background term

$$A^\ell_{\mathbf{s}}(t) = B^\ell_{\mathbf{s}}(t) + A0^\ell_{\mathbf{s}}. \tag{1}$$

Here $A0^\ell_{\mathbf{s}}$ is not necessarily uniform over the lattice grids. The dynamic term $B^\ell_{\mathbf{s}}(t)$ represents the component associated with repeat and near-repeat victimiza-

[1] With minor changes we can also consider e.g. the Dirichlet boundary conditions, which is more realistic.

tion, which will be discussed shortly. The initial data are given as $(n_{\mathbf{s}}^{\ell}(0), B_{\mathbf{s}}^{\ell}(0)) = (n0_{\mathbf{s}}^{\ell}, B0_{\mathbf{s}}^{\ell})$.

We assume that the Poisson clock advances according to a Poisson process with rate $D\ell^{-2}$, D an absolute constant independent of ℓ. On average, the time increment δt is the inverse of the rate

$$\delta t \cong \frac{\ell^2}{D}. \tag{2}$$

This is analogous to the Brownian scaling used in the DTS Model [76]. Suppose that the clock advances at time t^-. At time t, the system gets updated as follows:

Step 1. Every agent chooses to burglarize with the probability

$$p_{\mathbf{s}}^{\ell}(t) = 1 - e^{-\frac{A_{\mathbf{s}}^{\ell}(t^-)\ell^2}{D}} \cong A_{\mathbf{s}}^{\ell}(t^-)\delta t, \tag{3}$$

where $\mathbf{s}$ is his current location. This implies that burglary events occur roughly according to a Poisson process with the rate $A_{\mathbf{s}}^{\ell}(t^-)$.

Step 2. If an agent chooses to burglarize, he will be immediately removed from the system (representing the criminal fleeing with his trophy). If he chooses not to, he will jump from site $\mathbf{s}$ to one of the neighboring sites, say $\mathbf{k}$, with the probability proportional to the attractiveness of the target site

$$q_{\mathbf{s}\to\mathbf{k}}^{\ell}(t) = \frac{A_{\mathbf{k}}^{\ell}(t^-)}{T_{\mathbf{s}}^{\ell}(t^-)}, \tag{4}$$

where $T_{\mathbf{s}}^{\ell}(t) := \sum_{\mathbf{s}'\sim\mathbf{s}} A_{\mathbf{s}'}^{\ell}(t)$, and $\mathbf{s}' \sim \mathbf{s}$ indicates all of the neighboring sites of $\mathbf{s}$.

Step 3. The attractiveness field gets updated according to the repeat and near-repeat victimization and the broken-windows effect. These concepts in criminology and sociology have all been empirically observed [8, 25, 33]. The "broken windows" theory argues that the visible signs of past crimes are likely to create an environment that encourages further illegal activities [83]. The so-called repeat and near-repeat events refer to the phenomenon that residential burglars prefer to return to a previously burglarized house and its neighbors [23, 39, 40, 41, 75]. The repeat victimization is modeled by letting $B_{\mathbf{s}}^{\ell}$ depend upon previous burglary events at site $\mathbf{s}$. The attractiveness increases if a burglary event occurred on that site, and this increase has a finite lifetime. Let $E_{\mathbf{s}}^{\ell}(t)$ be the total number of burglary events that occurred at site $\mathbf{s}$ within this time step, then the repeat victimization can be modeled as

$$B_{\mathbf{s}}^{\ell}(t) = B_{\mathbf{s}}^{\ell}(t^-)\left(1 - \frac{\omega\ell^2}{D}\right) + \theta E_{\mathbf{s}}^{\ell}(t), \tag{5}$$

where ω and θ are absolute constants setting the speed of the decay and measuring the strength of the repeat victimization effect. The near-repeat victimization and broken windows effects are modeled by allowing $B_{\mathbf{s}}^{\ell}$ to spread in space from each house to its neighbors. To accomplish this, we modify (5) to read

$$B_{\mathbf{s}}^{\ell}(t) = \left[B_{\mathbf{s}}^{\ell}(t^{-}) + \frac{\eta}{4}\ell^{2}\Delta^{\ell}B_{\mathbf{s}'}^{\ell}(t^{-})\right]\left(1 - \frac{\omega\ell^{2}}{D}\right) + \theta E_{\mathbf{s}}^{\ell}(t), \tag{6}$$

where $\eta \in (0,1)$ is an absolute constant that measures the significance of neighborhood effects, and Δ^{ℓ} is the discrete spacial Laplace operator associated to the lattice grid, namely

$$\Delta^{\ell}B_{\mathbf{s}}^{\ell}(t) = \ell^{-2}\left(\sum_{\substack{\mathbf{s}' \\ \mathbf{s}' \sim \mathbf{s}}} B_{\mathbf{s}'}^{\ell}(t) - 4B_{\mathbf{s}}^{\ell}(t)\right).$$

Step 4. Let Γ be an absolute constant indicating the growth rate of criminal population. At each site with probability $\Gamma\ell^{2}/D$, a new agent will be replaced. We assume that ℓ is small enough such that $\Gamma\ell^{2}/D < 1$.

Figure 2.1.1 presents a visual summary of the above steps in the form of a flow chart.

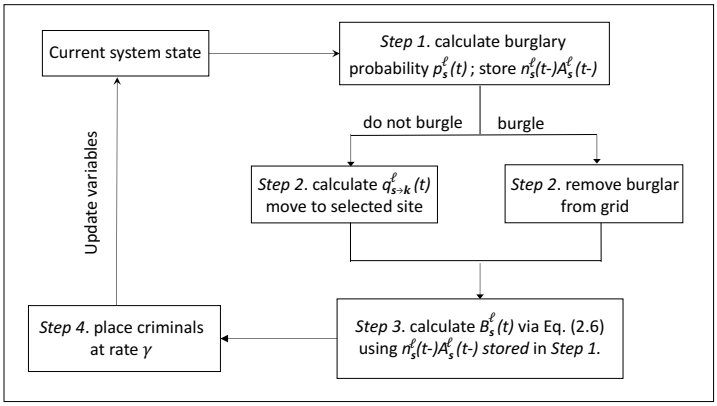

Flowchart summarizing the discrete model.

The spatially homogeneous equilibrium solutions are the same as in the DTS Model [76]. For simplicity from now on we always assume that $A0_{\mathbf{s}}^{\ell} \equiv A0$. Then the homogeneous equilibrium values can be deduced as

$$\bar{B} = \frac{\theta\Gamma}{\omega}, \quad \bar{n}^{\ell} = \frac{\Gamma\ell^{2}}{D\left(1 - e^{-\frac{\ell^{2}\bar{A}}{D}}\right)} \cong \frac{\Gamma}{\bar{A}}. \tag{7}$$

where $\bar{A} = \bar{B} + A0$,

2.1.2 Numerical simulations

To compare the Poisson-clock model and the DTS Model [76], we perform simulations of the attractiveness field $A^\ell_{\mathbf{s}}(t)$ in Figs. 1-3,. The parameters are mostly the equivalent of the parameters used to create the plots for the DTS Model [76] in Fig. 3, [76], and the same behavioral regimes are observed:

(1) Spatial homogeneity. In this regime, $A^\ell_{\mathbf{s}}(t)$ does not vary essentially in time or in space. Very few visible hotspots, that is, the accumulation of $A^\ell_{\mathbf{s}}(t)$ in time and in space, appear in the process.

(2) Dynamic hotspots. In this regime, hotspots form and are transient.

(3) Stationary hotspots. In this regime, hotspots will form and stay more or less stationary over time.

For all the simulations, the spatially homogeneous equilibrium value of the dynamic attractiveness $\bar{B}$ in (7) serves as a midpoint, and is shaded in green. A color key is given in the figures to document the false color map for the attractiveness. All the simulations were run with $L = 128$, $\ell = 1$, $\omega = 1/15$, $A0 = 1/30$, and the initial criminal number at each site $n0^\ell_{\mathbf{s}}$ is set be $\bar{n}^\ell$ on average[2]. In Figs. 1(c), 1(d), 3(a), and 3(b), we set $\Gamma = 0.0019q$, $\theta = 5.6/q$, $q = 1$, 10, 100, and 1000, respectively. The same is true of Figs. 2(c), 2(d), 3(c), and 3(d). As q increases, (7) implies that the initial criminal population and the criminal replacement rate both increase while the initial attractiveness field remains fixed.

Specific to the Poisson-clock model (Figs. 1(a), 1(b), 2(a), 2(b), and 3), we set $D = 100$. Specific to the DTS Model [76] (the remaining figures), we set $\delta t = 1/100$. Specific to the cases with zero hotspot formation (Figs. 1, Figs. 3(a) and (b)), we set $\eta = 0.2$ and $B0^\ell_{\mathbf{s}} \equiv \bar{B}$ for every $\mathbf{s} \in \mathscr{S}$. Specific to the cases with hotspot formation (the remaining figures), η is set to be 0.03, and $B0^\ell_{\mathbf{s}}$ is set to be $\bar{B}$ on every site except for 30 grid points randomly chosen a priori each gets increased by 0.002.

The same *finite size effects* as in the DTS Model [76] are observed, that is, the degree of hotspot 'transience' seems to depend on the total criminal population. The regimes of transient hotspots seem to appear associated with low or vanishing criminal numbers and low numbers of events, while the regimes of stationarity, including the stationary hotspots or homogeneity regimes, occur more likely with large numbers of criminals and burglary events.

2.2 Martingale formulation

For every t, we define $\big(B^\ell(t), n^\ell(t)\big) := \{\big(B^\ell_{\mathbf{s}}(t), n^\ell_{\mathbf{s}}(t)\big) : \mathbf{s} \in \mathscr{S}^\ell\}$, and similarly we can define the stochastic processes $n^\ell(t)$, $A^\ell(t)$, $p^\ell(t)$ and $E^\ell(t)$. associated with the Poisson-clock model. For $f^\ell := \{f^\ell_{\mathbf{s}} : \mathbf{s} \in \mathscr{S}^\ell\}$ and $g^\ell := \{g^\ell_{\mathbf{s}} : \mathbf{s} \in \mathscr{S}^\ell\}$, we define the discrete inner product and L^p norm over the lattice $\mathscr{S}^\ell$:

[2] More precisely, the criminal agents are assumed to be uniformly (randomly) distributed over the 128×128 grids, while $\sum_{\mathbf{s}\in\mathscr{S}^\ell} n0^\ell_{\mathbf{s}} = 128^2 \bar{n}^\ell$.

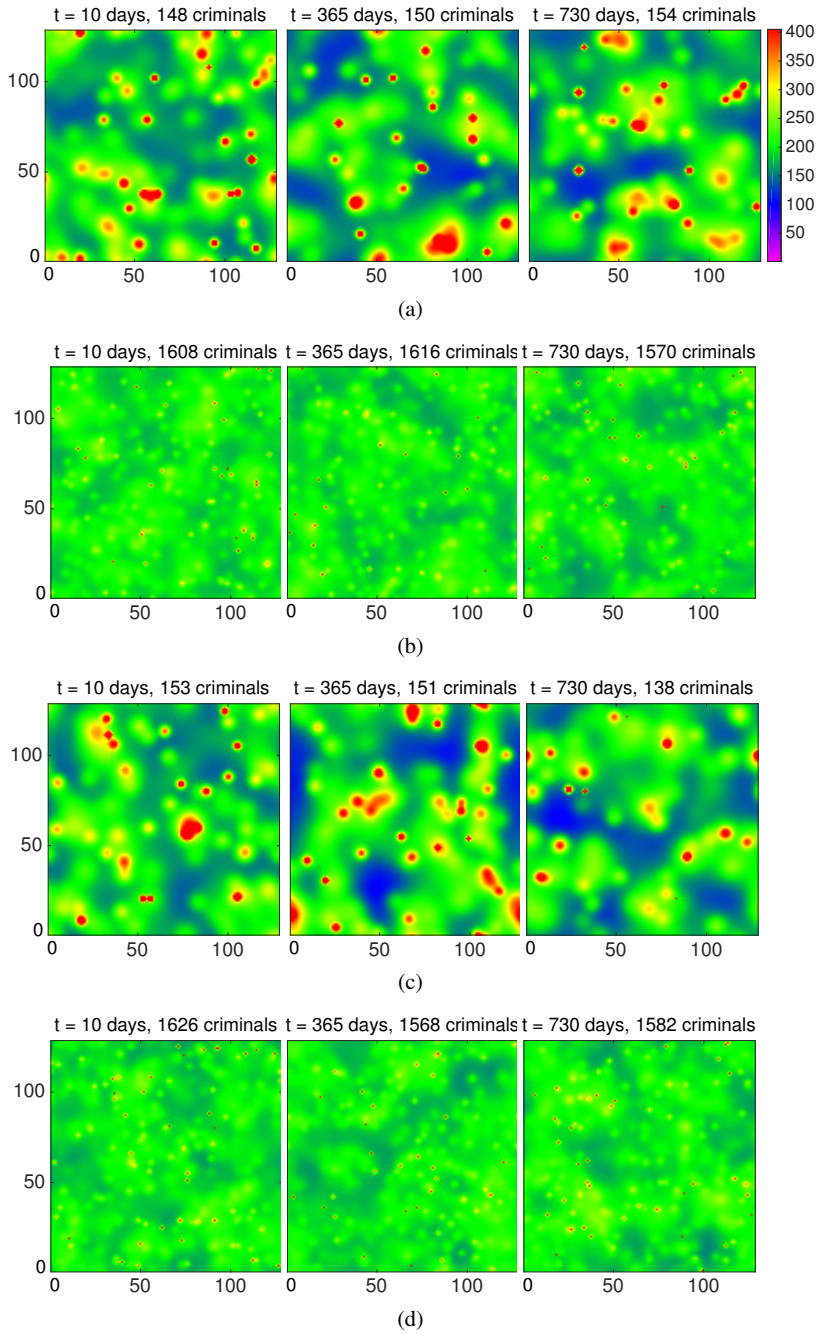

Fig. 1 Plot of the attractiveness $A_{\mathbf{s}}^{\ell}(t)$ for the discrete Poisson-clock model and the DTS Models [76]. For both models, The initial conditions (at $t = 0$) and parameters are taken to be $A0 = 1/30$, $B0_{\mathbf{s}}^{\ell} \equiv \bar{B}$, $n0_{\mathbf{s}}^{\ell} \cong \bar{n}^{\ell}$, $L = 128$, $\ell = 1$, $\omega = 1/15$, and $\eta = 0.2$. Specific to the Poisson-clock model (a) and (b), we set $D = 100$, $\Gamma = 0.0019q$, $\theta = 5.6/q$, $q = 1$ in (a), and $q = 10$ in (b). Specific to the DTS Model [76] (c) and (d), we set $\delta t = 1/100$, $\Gamma = 0.0019q$, $\theta = 5.6/q$, $q = 1$ in (c), and $q = 10$ in (d). (b) and (d) show the spatially homogeneous regimes. (a) and (c) show the dynamic hotspot regimes.

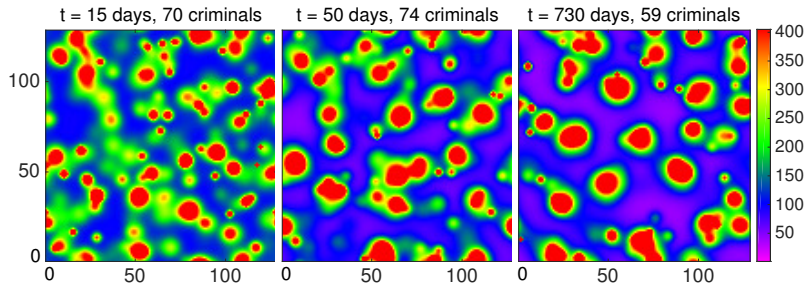

(a)

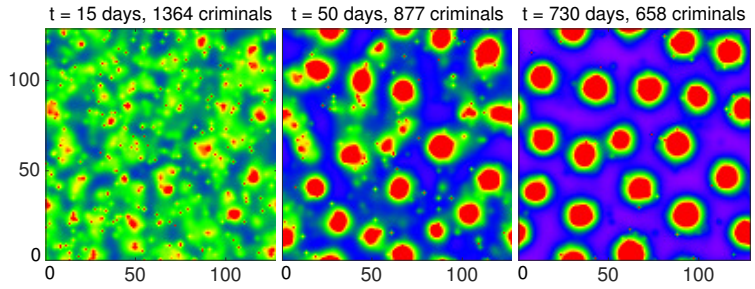

(b)

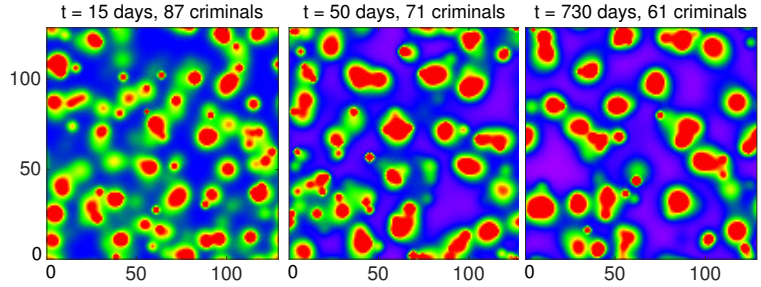

(c)

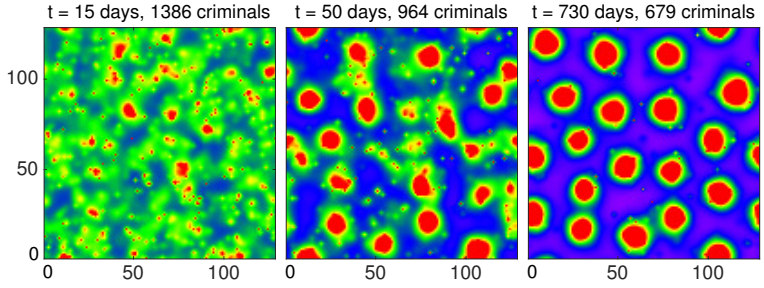

(d)

Fig. 2 Plot of the attractiveness $A_{\mathbf{s}}^{\ell}(t)$ for the discrete Poisson-clock model and the DTS Model [76]. For both models, The parameters and initial conditions (at $t = 0$) are taken to be $L = 128$, $\ell = 1$, $\omega = 1/15$, $\eta = 0.03$, $A0 = 1/30$, $n0_{\mathbf{s}}^{\ell} \cong \bar{n}^{\ell}$, and $B0^{\ell}$ is set to be $\bar{B}$ except for sites with slight perturbations. Specific to the Poisson-clock model (a) and (b), we set $D = 100$, $\Gamma = 0.0019q$, $\theta = 5.6/q$, $q = 1$ in (a), and $q = 10$ in (b). Specific to the DTS Model [76] (c) and (d), we set $\delta t = 1/100$, $\Gamma = 0.0019q$, $\theta = 5.6/q$, $q = 1$ in (c), and $q = 10$ in (d). (b) and (d) show the spatially homogeneous regimes. (a) and (c) show the dynamic hotspot regimes.

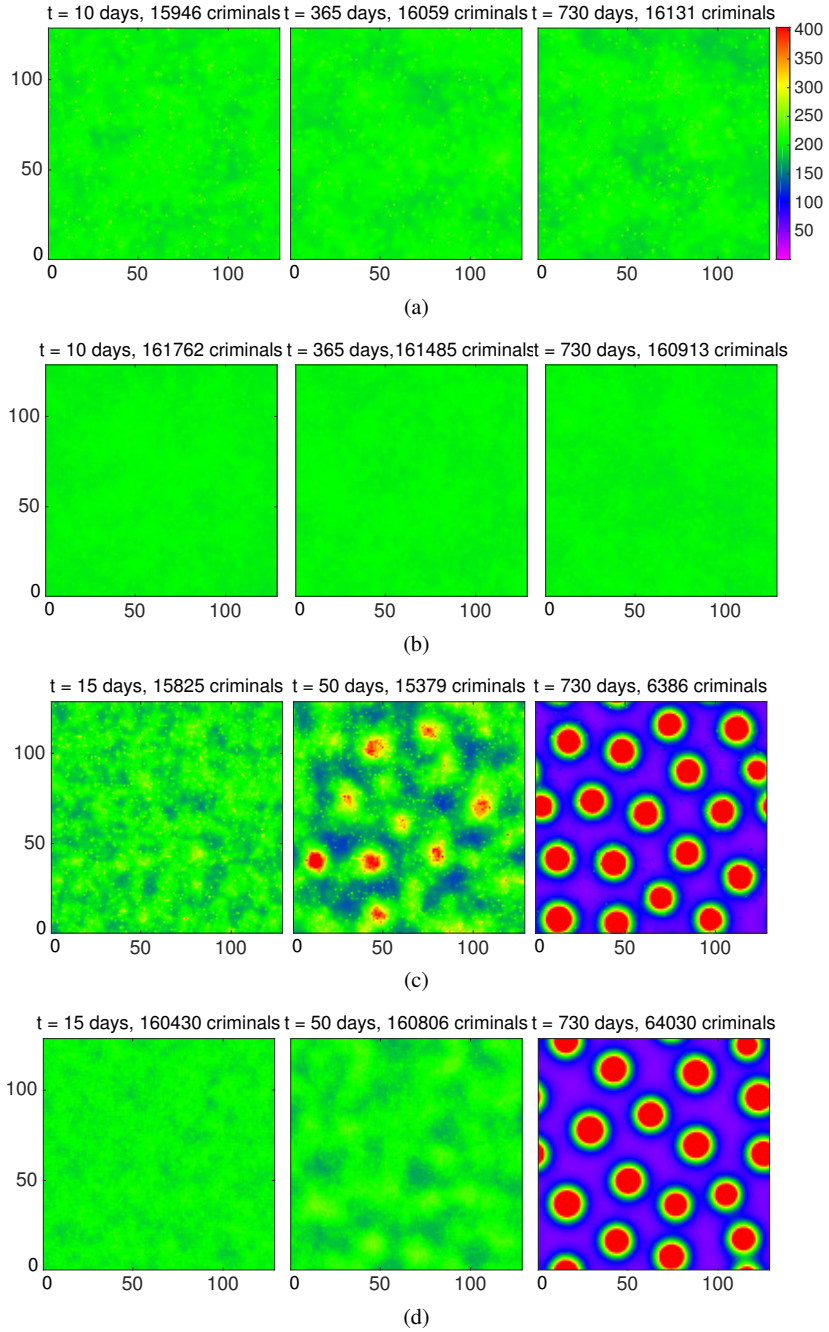

Fig. 3 Plot of the attractiveness $A^{\ell}_{\mathbf{s}}(t)$ for the discrete Poisson-clock model. For both regimes, the initial conditions (at $t = 0$) and parameters are taken to be $A0 = 1/30$, $n0^{\ell}_{\mathbf{s}} \cong \bar{n}^{\ell}$, $L = 128$, $\ell = 1$, $\omega = 1/15$, and $D = 100$. Specific to the spatially homogeneous regime (a) and (b), we set $B0^{\ell} \equiv \bar{B}$, $\eta = 0.2$, $\Gamma = 0.0019q$, $\theta = 5.6/q$, $q = 100$ in (a), and $q = 1000$ in (b). Specific to the dynamic hotspot regime (c) and (d), we set $\eta = 0.03$, $B0^{\ell}$ to be $\bar{B}$ except for sites with slight perturbations, $\Gamma = 0.0019q$, $\theta = 5.6/q$, $q = 100$ in (c), and $q = 1000$ in (d).

$$\left\langle f^\ell, g^\ell \right\rangle := \ell^2 \sum_{\mathbf{s}\in\mathscr{S}^\ell} f^\ell_{\mathbf{s}} g^\ell_{\mathbf{s}}, \quad \left| f^\ell \right|_p := \left(\ell^2 \sum_{\mathbf{s}\in\mathscr{S}^\ell} \left| f^\ell_{\mathbf{s}} \right|^p \right)^{1/p}, \quad p \geq 1.$$

Let $\phi^\ell = \{\phi^\ell_{\mathbf{s}} : \mathbf{s} \in \mathscr{S}^\ell\}$ be an arbitrary stationary scalar field, we define

$$\left\langle \left(B^\ell(t), n^\ell(t) \right), \phi^\ell \right\rangle := \left(\left\langle B^\ell(t), \phi^\ell \right\rangle, \left\langle n^\ell(t), \phi^\ell \right\rangle \right). \tag{8}$$

$\left\langle \left(B^\ell(t), n^\ell(t) \right), \phi^\ell \right\rangle$ is a Markov pure jump process with state space $\mathbb{R}^2$. Hence a martingale approach is applicable (e.g. [14, 15, 44, 51, 79]). The martingale formulation of the process can be derived based on the infinitesimal parameters. The components of the infinitesimal mean vector and diagonal components of the infinitesimal covariance matrix of $\left\langle \left(B^\ell(t), n^\ell(t) \right), \phi^\ell \right\rangle$ are denoted as follows:

$$\begin{cases} \text{infinitesimal mean for attractiveness } \mathscr{G}^\ell_1 \left(\left\langle \left(B^\ell(t), n^\ell(t) \right), \phi^\ell \right\rangle \right), \\ \text{infinitesimal mean for criminal distribution } \mathscr{G}^\ell_2 \left(\left\langle \left(B^\ell(t), n^\ell(t) \right), \phi^\ell \right\rangle \right), \\ \text{infinitesimal variance for attractiveness } \mathscr{V}^\ell_1 \left(\left\langle \left(B^\ell(t), n^\ell(t) \right), \phi^\ell \right\rangle \right), \\ \text{infinitesimal variance for criminal distribution } \mathscr{V}^\ell_2 \left(\left\langle \left(B^\ell(t), n^\ell(t) \right), \phi^\ell \right\rangle \right). \end{cases}$$

Thus we have the following martingale formulation for $\left\langle \left(B^\ell(t), n^\ell(t) \right), \phi^\ell \right\rangle$:

Theorem 2.1 *For each fixed ℓ, before the possible blow-up time, the stochastic process $\left\langle \left(B^\ell(t), n^\ell(t) \right), \phi^\ell \right\rangle$ can be written as*

$$\begin{cases} \left\langle B^\ell(t), \phi^\ell \right\rangle = & \left\langle B0^\ell, \phi^\ell \right\rangle + \int_0^t \mathscr{G}^\ell_1 \left(\left\langle \left(B^\ell(s), n^\ell(s) \right), \phi^\ell \right\rangle \right) ds \\ & + \mathscr{M}^\ell_1 \left(\left\langle \left(B^\ell(t), n^\ell(t) \right), \phi^\ell \right\rangle \right), \\ \left\langle n^\ell(t), \phi^\ell \right\rangle = & \left\langle n0^\ell, \phi^\ell \right\rangle + \int_0^t \mathscr{G}^\ell_2 \left(\left\langle \left(B^\ell(s), n^\ell(s) \right), \phi^\ell \right\rangle \right) ds \\ & + \mathscr{M}^\ell_2 \left(\left\langle \left(B^\ell(t), n^\ell(t) \right), \phi^\ell \right\rangle \right). \end{cases} \tag{9}$$

where $\mathscr{M}^\ell_i \left(\left\langle \left(B^\ell(t), n^\ell(t) \right), \phi^\ell \right\rangle \right)$, $i = 1, 2$, are martingales starting at $t = 0$ as zeros, whose variances can be characterized by the infinitesimal variances:

$$Var\left(\mathscr{M}^\ell_i \left(\left\langle \left(B^\ell(t), n^\ell(t) \right), \phi^\ell \right\rangle \right) \right) = \int_0^t \mathbb{E} \left[\mathscr{V}^\ell_i \left(\left\langle \left(B^\ell(s), n^\ell(s) \right), \phi^\ell \right\rangle \right) \right] ds, \tag{10}$$

where $i = 1, 2$. Moreover for the infinitesimal means and variances we have

$$\begin{aligned} & \mathscr{G}^\ell_1 \left(\left\langle \left(B^\ell(t), n^\ell(t) \right), \phi^\ell \right\rangle \right) \\ & = \left\langle \left(1 - \frac{\omega \ell^2}{D} \right) \frac{\eta D}{4} \Delta^\ell B^\ell(t) - \omega B^\ell(t) + D\theta \ell^{-2} p^\ell(t) n^\ell(t), \phi^\ell \right\rangle, \end{aligned} \tag{11}$$

$$\mathscr{G}_2^\ell\left(\left\langle\left(B^\ell(t),n^\ell(t)\right),\phi^\ell\right\rangle\right)$$
$$=\ell^2\sum_{s\in\mathscr{S}^\ell}\left[D\ell^{-2}\left(A_s^\ell(t)\sum_{\substack{s'\\ s'\sim s}}\frac{n_{s'}^\ell(t)\left(1-p_{s'}^\ell(t)\right)}{T_{s'}^\ell(t)}-n_s^\ell(t)\right)+\Gamma\right]\phi_s^\ell, \tag{12}$$
$$\mathscr{V}_1^\ell\left(\left\langle\left(B^\ell(t),n^\ell(t)\right),\phi^\ell\right\rangle\right)$$
$$=\frac{\ell^2}{D}\left(\mathscr{G}_1^\ell\left(\left\langle\left(B^\ell(t),n^\ell(t)\right),\phi^\ell\right\rangle\right)\right)^2$$
$$+D\theta^2\left\langle n^\ell(t)p^\ell(t)(1-p^\ell(t)),\left(\phi^\ell\right)^2\right\rangle, \tag{13}$$
$$\mathscr{V}_2^\ell\left(\left\langle\left(B^\ell(t),n^\ell(t)\right),\phi^\ell\right\rangle\right)$$
$$=\frac{\ell^2}{D}\left(\mathscr{G}_2^\ell\left(\left\langle\left(B^\ell(t),n^\ell(t)\right),\phi^\ell\right\rangle\right)\right)^2+\ell^2\Gamma\left(1-\frac{\Gamma\ell^2}{D}\right)\left|\phi^\ell\right|_2^2$$
$$+D\left\langle n^\ell(t)\left(1-p^\ell(t)\right),p^\ell(t)f^\ell(t)+g^\ell(t)\right\rangle, \tag{14}$$

where

$$f_s^\ell(t)=\left(\sum_{\substack{s'\\ s'\sim s}}\phi_{s'}\frac{A_{s'}^\ell(t)}{T_s^\ell(t)}\right)^2,\qquad g_s^\ell(t)=\ell^2\sum_{\substack{s'\\ s'\sim s}}\frac{A_{s'}^\ell(t)}{T_s^\ell(t)}\left(\sum_{\substack{s''\\ s''\neq s'\\ s''\sim s}}\nabla_{s'\to s''}^\ell\phi_{s'}^\ell\frac{A_{s''}^\ell(t)}{T_s^\ell(t)}\right)^2. \tag{15}$$

Here $\nabla_{s'\to s''}^\ell\phi_{s'}^\ell$ denotes the discrete directional derivative from s' pointing towards s'', that is, $\nabla_{s'\to s''}^\ell\phi_{s'}^\ell=\left(\phi_{s'}^\ell-\phi_{s''}^\ell\right)/\ell$.

The proof of Theorem 2.1 is in the Appendix.

2.3 Continuum model

The martingale formulation (9) implies that the process $\left\langle\left(B^\ell(t),n^\ell(t)\right),\phi^\ell\right\rangle$ is characterized by infinitesimal means and variances. The former gives the expected behavior and the latter the variance of the trajectories of the evolution. Thus the process can be viewed as the sum of differential equations and random fluctuations. From (13) and (14) we infer that the infinitesimal variances have a lower order of magnitude than ℓ, that is:

$$
\begin{aligned}
&\mathscr{V}_1^\ell\left(\left\langle\left(B^\ell(t),n^\ell(t)\right),\phi^\ell\right\rangle\right)\\
\cong&\frac{\ell^2}{D}\left(\mathscr{G}_1^\ell\left(\left\langle\left(B^\ell(t),n^\ell(t)\right),\phi^\ell\right\rangle\right)\right)^2+\ell^2\theta^2\left\langle n^\ell(t)A^\ell(t),\left(\phi^\ell\right)^2\right\rangle\\
\cong&O(\ell^2),
\end{aligned}
\tag{16}
$$

$$
\begin{aligned}
&\mathscr{V}_2^\ell\left(\left\langle\left(B^\ell(t),n^\ell(t)\right),\phi^\ell\right\rangle\right)\\
\cong&\frac{\ell^2}{D}\left(\mathscr{G}_2^\ell\left(\left\langle\left(B^\ell(t),n^\ell(t)\right),\phi^\ell\right\rangle\right)\right)^2+\ell^2\Gamma\left|\phi^\ell\right|_2^2\\
&+D\ell^2\left\langle n^\ell(t),\frac{1}{D}A^\ell(t)f^\ell(t)+g^\ell(t)\ell^{-2}\right\rangle\\
\cong&O(\ell^2).
\end{aligned}
\tag{17}
$$

Thus for ℓ small, it is reasonable to set the continuum version of the differential equations as a continuum model. Let $n(\mathbf{x},t)$, $A(\mathbf{x},t)$, and $B(\mathbf{x},t)$, $\mathbf{x}\in\mathscr{D}$ be the continuum versions of $n_{\mathbf{s}}^\ell(t)$, $A_{\mathbf{s}}^\ell(t)$, and $B_{\mathbf{s}}^\ell(t)$, we have

$$
\begin{cases}
\dfrac{\partial B}{\partial t}=\dfrac{\eta D}{4}\Delta B-\omega B+\theta nA,\\[2ex]
\dfrac{\partial n}{\partial t}=\dfrac{D}{4}\nabla\cdot\left(\nabla n-\dfrac{2n}{A}\nabla A\right)-nA+\Gamma,\\[2ex]
n(0)=n0,B(0)=B0.
\end{cases}
\tag{18}
$$

We note that (18) and the continuum DTS Model [76] ((3.2) and (3.5) in [76]) are the same. The derivation of (18) is similar to that of the hydrodynamic limit of interacting particle systems [19, 30, 44, 45, 69, 70, 79, 80].

We verify the validity of the continuum model through simulations. We use the same algorithm as the continuum DTS Model [76] ((3.11)-(3.13) in [76]). Fig. 4 shows example output of the attractiveness $A(\mathbf{x},t)$ in the cases of hotspot formation. The same color key is used as in Fig. 1. From (18) we infer that the parameters and data used to create Figs. 2(a), 2(b), 3(c), and 3(d) give rise to the same continuum attractiveness field. Hence we only display the output once here in Fig. 4. As for the case of zero hotspot formation, the parameters and data used to create Figs. 1(a), 1(b), 3(a), and 3(b) give rise to the same continuum attractiveness field, which is the equilibrium as the the system stays at the equilibrium with equilibrium initial data.

As was observed in the DTS Model [76], the regimes of dynamic hotspots are absent in the continuum simulations. As the total criminal population decreases, distinctions between the behavioral regimes of the discrete and continuum simulations increase.

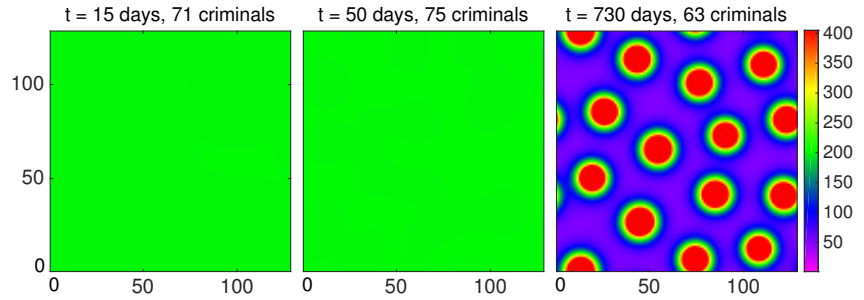

Fig. 4 Output of the attractiveness $A(\mathbf{x},t)$ for the continuum Poisson-clock model with hotspot formation. The parameters and data are the equivalent of the discrete parameters used in Figs. 2, 3(c) and 3(d).

3 Mathematical analysis of the *finite size effects*

Hotspot transience is well documented in real crime statistics. It would be useful if we could guess the parameters of the model from observed pattern formation. The *finite size effects* are closely related to the degree of hotspot transience. Therefore, through the observation of the hotspot transience, we could estimate the number of criminals. This number is normally difficult to predict. To analyze the *finite size effects* quantitatively, we build a mathematical framework to quantify the relevant pattern formation. We propose a theory for the *finite size effects* based on a scaling property of the martingale formulation. Our conjecture is supported by qualitative and quantitative simulations.

3.1 Quantification of the pattern formation

3.1.1 Statistics of degree of the hotspot transience

We construct the following statistics to measure the degree of hotspot transience.

(i) Relative Fisher information relative to the uniform measure over $\mathscr{S}^\ell$, logarithm mean type (See Appendix [11]):

$$\mathscr{I}^\ell(t) := \ell^{-2} \sum_{\mathbf{s}\in\mathscr{S}} \left(A^\ell_{\mathbf{s}}(t) - A^\ell_{\mathbf{s}'}(t)\right)\left(\log A^\ell_{\mathbf{s}}(t) - \log A^\ell_{\mathbf{s}}(t)\right). \tag{19}$$

As suggested in [20, 21, 22], the Fisher information is particularly suitable to measure the entropy of diffusion processes, which fits with the dynamics of the attractiveness.

(ii) Rate of change of $A^\ell(t)$ over time in the discrete L^p norm, $p \geq 1$. For a fixed time increment $\Delta t > 0$, we define the L^p-area rate of change as:

$$\delta_p^\ell(t) := \left| A^\ell(t+\Delta t) - A^\ell(t) \right|_p . \tag{20}$$

(iii) Rate of change of the total area of certain types of regions. We focus on the regions with attractiveness higher than $2\bar{A}$ (red regions). For these regions, we define the relative overlapping area $\mathscr{O}^\ell(t)$ and non-overlapping area $\mathscr{N}^\ell(t)$ as follows:

$$\mathscr{O}^\ell(t) := \frac{1}{A_R^\ell} \sum_{\substack{\mathbf{s}\in\mathscr{S}^\ell \\ A_{\mathbf{s}}^\ell(t)\geq 2\bar{A} \\ A_{\mathbf{s}}^\ell(t+\Delta t)\geq 2\bar{A}}} \mathbf{1}(\mathbf{s}) \tag{21}$$

$$\mathscr{N}^\ell(t) := \frac{1}{A_R^\ell} \left[\sum_{\substack{\mathbf{s}\in\mathscr{S}^\ell \\ A_{\mathbf{s}}^\ell(t+\Delta t)\geq 2\bar{A}}} \mathbf{1}(\mathbf{s}) + \sum_{\substack{\mathbf{s}\in\mathscr{S}^\ell \\ A_{\mathbf{s}}^\ell(t)\geq 2\bar{A}}} \mathbf{1}(\mathbf{s}) \right] - 2\mathscr{O}^\ell(t), \tag{22}$$

where $\mathbf{1}(\mathbf{s})$ is an indicator function, and A_R^ℓ is the renormalization:

$$A_R^\ell = \sum_{\substack{\mathbf{s}\in\mathscr{S}^\ell \\ A_{\mathbf{s}}^\ell(t)\geq 2\bar{A}}} \mathbf{1}(\mathbf{s}) \tag{23}$$

As for the continuum model, in a very similar way we can define all the above quantities, and we denote them as $\mathscr{I}(t)$, $\delta_p(t)$, $\mathscr{O}(t)$, and $\mathscr{N}(t)$.

3.1.2 Numerical simulations

Example output of direct simulations for (19)-(22) can be seen in Figs. 5-7. All the simulations are run with $\Delta t = 10$, $t \in [0, 730]$, and $p = 1$. Moreover, the blue, magenta, black and red lines show results with increasing values of q and thus increasing criminal population. Figs. 5(a) and 6(a) show results with zero hotspot formation, and the blue, magenta, black, and red lines represent results with the simulations in Figs. 1(a), 1(b), 3(a), 3(b), respectively. Figs. 5(b), 6(b) and 7 show results with hotspot formation, and the blue, magenta, black, red, and green lines represent results with the simulations in Figs. 2(a), 2(b), 3(c), 3(d), and 4, respectively.

The simulation output shows that a larger degree of hotspot transience appears with a smaller criminal population. Also the continuum simulations have the lowest degree of hotspot transience. The peaks in Figs. 6(b), 7(a) and 7(b) correspond to the initial emergence of the hotspots in the discrete and continuum models. During the emergence period the statistics increase as the hotspots form, and decrease and stabilize (or directly stabilize) as the hotspots stabilize. The same simulation results are also observed over other random paths. To conclude, the output matches well with the qualitative simulations in Figs. 1-4, which suggests that the above statistics are suitably chosen.

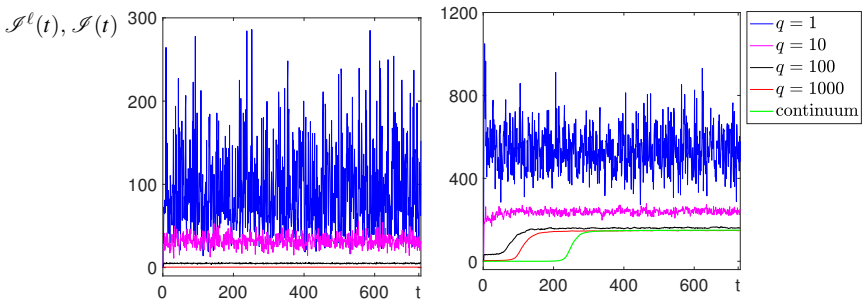

(a) (b)

Fig. 5 Examples of the relative Fisher information $\mathscr{I}^{\ell}(t)$ and $\mathscr{I}(t)$ in the cases of zero hotspot formation and hotspot formation. (a) shows results with the cases of zero hotspot formation, and the blue, magenta, black and red lines represent the statistics of the discrete models plotted in Figs. 1(a), 1(b), 3(a), and 3(b), respectively. (b) shows results with the cases of hotspot formation, and the blue, magenta, black, red and green lines show results with the simulations in Figs. 2(a), 2(b), 3(c), 3(d), and 4 respectively.

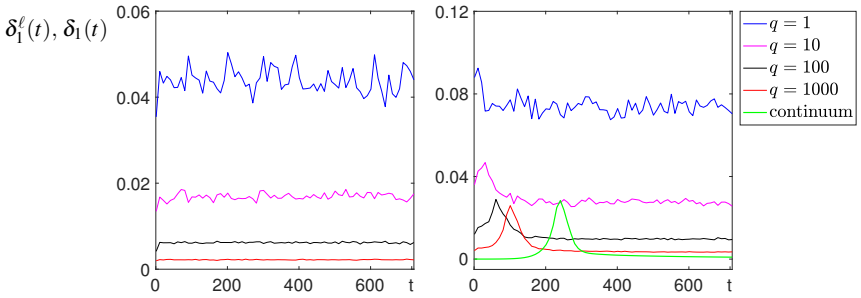

(a) (b)

Fig. 6 Examples of the L^1-area rate of change $\delta_1^{\ell}(t)$ and $\delta_1(t)$ in the cases of zero hotspot formation and hotspot formation. (a) shows results with zero hotspot formation, and the blue, magenta, black and red lines represent the statistics of the discrete models plotted in Figs. 1(a), 1(b), 3(a), and 3(b), respectively. (b) shows results with hotspot formation, and the blue, magenta, black, red and green lines show results with the simulations in Figs. 2(a), 2(b), 3(c), 3(d), and Fig. 4, respectively.

3.2 Theory of the finite size effects

With quantification of the degree of hotspot transience, we analyze the *finite size effects* mathematically.

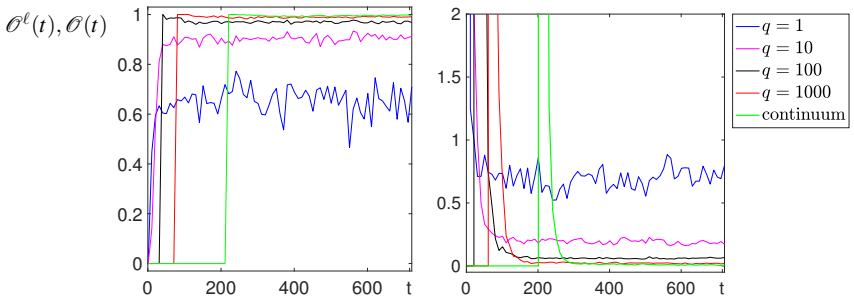

(a) (b)

Fig. 7 Examples of the relative overlapping and non-overlapping area, $\mathscr{O}^\ell(t)$, $\mathscr{O}(t)$, $\mathscr{N}^\ell(t)$ and $\mathscr{N}(t)$ with hotspot formation. The blue, magenta, black, red, and green lines show results with the simulations in Figs. 2(a), 2(b), 3(c), 3(d), and Fig. 4 respectively.

3.2.1 Scaling property of the stochastic component

We study a scaling property related to the total criminal population. Specifically we vary the initial criminal number, the repeat victimization strength θ, and the replacement rate Γ. Fixing $\Theta > 0$, $\mathfrak{d} > 0$, for $q \in (0, D/\ell^2\mathfrak{d})$, we consider the discrete model with parameters and initial data scaled in a certain way:

$$\left(B^{\ell,(q)}(t), n^{\ell,(q)}(t)\right) := \left(B^\ell(t), n^\ell(t)\right)\Big|_{B0^\ell \cong \bar{\mathfrak{B}},\ n0^\ell \cong q\bar{\mathfrak{n}}^\ell,\ \theta = \frac{\Theta}{q},\ \Gamma = q\mathfrak{d}}, \tag{24}$$

where $\bar{\mathfrak{B}}$, $\bar{\mathfrak{n}}^\ell$ are the homogeneous equilibrium values as in (7) with $\theta = \Theta$ and $\Gamma = \mathfrak{d}$:

$$\bar{\mathfrak{B}} = \frac{\Theta\mathfrak{d}}{\omega}, \quad \bar{\mathfrak{n}}^\ell = \frac{\mathfrak{d}\ell^2}{D\left(1 - e^{-\ell^2(\bar{\mathfrak{B}} + A0)D^{-1}}\right)} \cong \frac{\mathfrak{d}}{\bar{\mathfrak{B}} + A0}. \tag{25}$$

As q increases, the initial criminal population and the criminal replacement rate both increase while the initial attractiveness field remains fixed. Applying (9) and (10) to $\left(B^{\ell,(q)}(t), n^{\ell,(q)}(t)\right)$ over a small time step δt we obtain

$$\begin{cases} \left\langle B^{\ell,(q)}(t+\delta t), \phi^\ell \right\rangle = \left\langle B^{\ell,(q)}(t), \phi^\ell \right\rangle + \mathscr{G}_1^{\ell,(q)}\left(t, \phi^\ell\right)\delta t + \mathscr{M}_1^{\ell,(q)}\left(t, \phi^\ell\right), \\ \left\langle n^{\ell,(q)}(t+\delta t), \phi^\ell \right\rangle = \left\langle n^{\ell,(q)}(t), \phi^\ell \right\rangle + \mathscr{G}_2^{\ell,(q)}\left(t, \phi^\ell\right)\delta t + \mathscr{M}_2^{\ell,(q)}\left(t, \phi^\ell\right), \end{cases} \tag{26}$$

where $\mathscr{G}_i^{\ell,(q)}(t, \phi^\ell)$ are the short notations for $\mathscr{G}_i^\ell\left(\left\langle\left(B^{\ell,(q)}(t), n^{\ell,(q)}(t)\right), \phi^\ell\right\rangle\right)$, and $\mathscr{M}_i^{\ell,(q)}\left(t, \phi^\ell\right)$ for $\mathscr{M}_i^\ell\left(\left\langle\left(B^{\ell,(q)}(t), n^{\ell,(q)}(t)\right), \phi^\ell\right\rangle\right)$, $i = 1, 2$. By (10) we obtain the standard deviation of the stochastic component

$$\sqrt{\mathrm{Var}\left(\mathscr{M}_i^{\ell,(q)}(t,\phi^\ell)\right)} \cong \sqrt{\mathbb{E}\left[\mathscr{V}_i^{\ell,(q)}(t,\phi^\ell)\right]\delta t}, \quad i=1,2, \tag{27}$$

where $\mathscr{V}_i^{\ell,(q)}(t,\phi^\ell)$'s are the short nations for $\mathscr{V}_i^\ell\left(\left\langle\left(B^{\ell,(q)}(t),n^{\ell,(q)}(t)\right),\phi^\ell\right\rangle\right)$, $i=$ 1, 2. This implies that the infinitesimal variances are the key to estimate deviation of the discrete model from the deterministic component.

We analyze the infinitesimal variance for attractiveness. By (11) and (13) we rewrite the infinitesimal variance as the summation of two components

$$\mathscr{V}_1^{\ell,(q)}\left(t,\phi^\ell\right) = \mathscr{V}_{1,1}^{\ell,(q)}\left(t,\phi^\ell\right) + \frac{1}{q}\mathscr{V}_{1,2}^{\ell,(q)}\left(t,\phi^\ell\right), \tag{28}$$

where

$$\begin{aligned}&\mathscr{V}_{1,1}^{\ell,(q)}\left(t,\phi^\ell\right)\\ &\cong \frac{\ell^2}{D}\left(\left\langle\frac{\eta D}{4}\Delta^\ell B^{\ell,(q)}(t)-\omega B^{\ell,(q)}(t)+\frac{\Theta}{q}\left(B^{\ell,(q)}(t)+A0\right)n^{\ell,(q)}(t),\phi^\ell\right\rangle\right)^2,\end{aligned} \tag{29}$$

and

$$\mathscr{V}_{1,2}^{\ell,(q)}\left(t,\phi^\ell\right) \cong q\ell^2\Theta^2\left\langle n^{\ell,(q)}(t)\left(B^{\ell,(q)}(t)+A0\right),\left(\phi^\ell\right)^2\right\rangle. \tag{30}$$

We perform estimates at the first time step. At time zero, from (29), (30) and (25) we infer that the two components are actually independent of q, namely

$$\mathscr{V}_{1,1}^{\ell,(q)}\left(0,\phi^\ell\right) = \frac{\ell^2}{D}\left(\left\langle-\omega\bar{\mathfrak{B}}+\Theta\left(\bar{\mathfrak{B}}+A0\right)\bar{\mathfrak{n}}^\ell,\phi^\ell\right\rangle\right)^2 = 0, \tag{31}$$

and

$$\mathscr{V}_{1,2}^{\ell,(q)}\left(0,\phi^\ell\right) = \ell^2\Theta^2\left\langle\bar{\mathfrak{n}}^\ell\left(\bar{\mathfrak{B}}+A0\right),\left(\phi^\ell\right)^2\right\rangle = \ell^2\Theta^2\mathfrak{b}\left|\phi^\ell\right|_2^2. \tag{32}$$

This together with (28) implies that at time zero we have

$$\mathscr{V}_1^{\ell,(q)}\left(0,\phi^\ell\right) \equiv q^{-1}\ell^2\Theta^2\mathfrak{b}\left|\phi^\ell\right|_2^2. \tag{33}$$

Thus we infer that the infinitesimal variance for the attractiveness is inversely proportional to q:

$$\mathscr{V}_1^{\ell,(q)}\left(0,\phi^\ell\right) \propto q^{-1}. \tag{34}$$

This implies that for $0<q<\tilde{q}<D\mathfrak{b}/\ell^2$, we have

$$\mathscr{V}_1^{\ell,(q)}\left(0,\phi^\ell\right) > \mathscr{V}_1^{\ell,(\tilde{q})}\left(0,\phi^\ell\right). \tag{35}$$

This together with (27) implies that at the first time step we have

$$\mathrm{Var}\left(\mathscr{M}_1^{\ell,(q)}\left(\delta t,\phi^\ell\right)\right) > \mathrm{Var}\left(\mathscr{M}_1^{\ell,(\tilde{q})}\left(\delta t,\phi^\ell\right)\right). \tag{36}$$

To conclude at the first time step a smaller value of q leads to a larger deviation of $B^{\ell,(q)}(t)$ from the deterministic component, and hence the hotspots develop temporal transience in the discrete attractiveness simulations. We conjecture that (35) remains to be true in later times, namely,

$$\mathscr{V}_1^{\ell,(q)}\left(t,\phi^\ell\right) > \mathscr{V}_1^{\ell,(\tilde{q})}\left(t,\phi^\ell\right), \text{ for } 0<q<\tilde{q}<\frac{D\mathfrak{b}}{\ell^2} \text{ and } t>0. \tag{37}$$

To conclude, the scaling property of the martingale formulation related to the criminal population possibly leads to the *finite size effects*.

3.2.2 Numerical simulations

We perform direct simulations of the infinitesimal standard deviation for the attractiveness, $\sqrt{\mathscr{V}_1^{\ell,(q)}(t)}$, to check the validity of (37). Example output can be seen in Figure. 8. The test function is chosen to be

$$\phi^\ell(\mathbf{x}) = 1 + sin(\mathbf{x}_1)sin(\mathbf{x}_2)/20. \tag{38}$$

Fig. 8(a) shows results in the cases with no hotspot. The blue, magenta, black, and red lines show results with the simulations in Figs. 1(a), 1(b), 3(a), and 3(b), respectively. Fig. 8(b) shows results with hotspot formation. The blue, magenta, black and red lines represent results with the simulations in Figs 2(a), 2(b), 3(c), and 3(d), respectively. The same simulation results are also observed over other random paths. The output of the simulations supports our previous conjecture as in (37).

Furthermore, in Fig. 9 we check whether (34) is valid for later times:

$$\mathscr{V}_1^{\ell,(q)}\left(t,\phi^\ell\right) \cong \frac{1}{q}\ell^2\Theta^2\mathfrak{b}\left|\phi^\ell\right|_2^2, \quad t>0. \tag{39}$$

Taking the average of both sides of (39) over the time period $[0,T]$, we obtain

$$\frac{1}{T}\int_0^T \mathscr{V}_1^{\ell,(q)}\left(t,\phi^\ell\right)dt \cong \frac{1}{q}\ell^2\Theta^2\mathfrak{b}\left|\phi^\ell\right|_2^2. \tag{40}$$

Fig. 9 shows the log-log plot of (40). The lines show the theoretical scaling with slope -1 and the x-intercept $\ell^2\Theta^2\mathfrak{b}\left|\phi^\ell\right|_2^2$. The points show the true scaling with the coordinates as:

$$x=\log q,\ y=\log\left(\frac{1}{T}\int_0^T \mathscr{V}_1^{\ell,(q)}\left(t,\phi^\ell\right)dt\right), \quad q=1,10,100,1000. \tag{41}$$

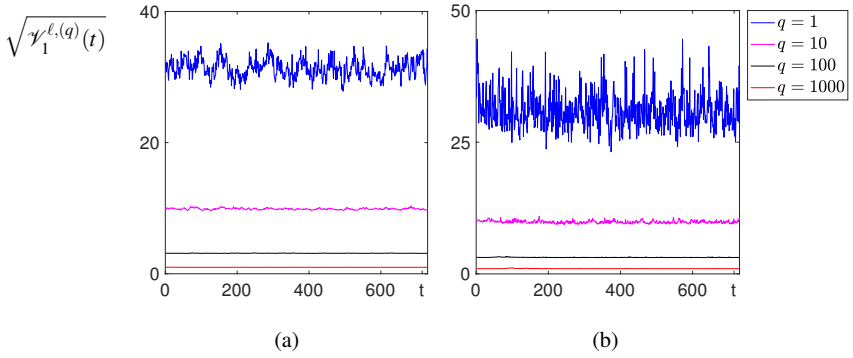

Fig. 8 Examples of the infinitesimal standard deviation for attractiveness, $\sqrt{\mathscr{V}_1^{\ell,(q)}(t)}$, for both zero hotspot formation and hotspot formation. (a) shows results with no hotspot, and the blue, magenta, black and red lines show results with the simulations in Figs. 1(a), 1(b), 3(a), and 3(b), respectively. (b) shows results with hotspot formation, and the blue, magenta, black and red lines show results with the simulations in Figs. 2(a), 2(b), 3(c), and 3(d), respectively.

The output shows that all the points fall onto the straight lines. This indicates stability of the Poisson-clock model with equilibrium initial value, which further indicates validity of the model.

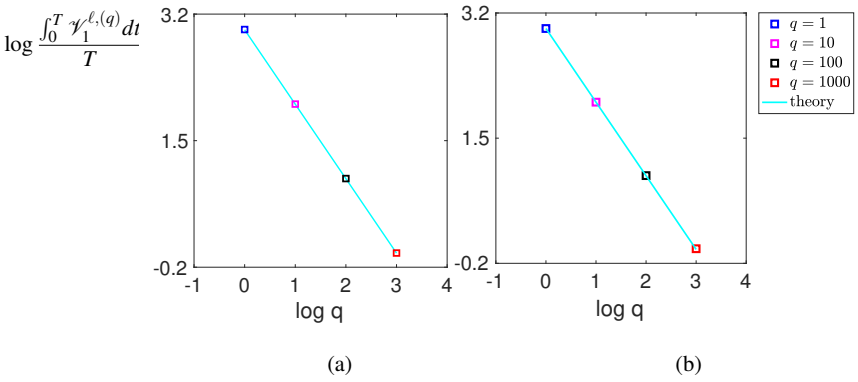

Fig. 9 Comparison of log-log plot of the theoretical and true scaling for both zero hotspot formation and hotspot formation. The straight lines show the theoretical scaling with slope -1 and the x-intercept $\ell^2\Theta^2\mathfrak{d}\left|\phi^\ell\right|_2^2 \cong 2.9892$. The points show the true scaling. (a) shows results with no hotspot, and the points with x-axis as 0, 1, 2, and 3 show results with the simulations of the blue, magenta, black and red lines in Fig. 8 (a), respectively. (b) shows results with hotspot formation, and the points with x-axis as 0, 1, 2, and 3 show results with the simulations of the blue, magenta, black and red lines in Fig. 8 (b), respectively.

4 Conclusion

In this paper, we apply the Poisson clock to the agent-based residential burglary DTS Model [76]. The time increments are exponentially distributed random variables, which are more suitable to model random arrivals. This is a Markov pure jump process, and a martingale approach is applicable. A martingale formulation is derived which consists of a deterministic and a stochastic component. It provides us with a tool to study both the statistical and stochastic features of the process. The model thus obtained is a stochastic-statistical residential burglary model (SSRB Model).

The deterministic part yields a continuum model. It is the same as the continuum version of the DTS Model [76]. We find that the continuum SSRB Model is a good approximation of the discrete SSRB Model under the circumstance of a large number of criminals. Moreover, for the *finite size effects*, we build statistics to quantify the relevant pattern formation, and find a theoretical explanation using a scaling property of the stochastic component. That is, as the criminal population decreases, the stochastic component increases in size, which leads to a larger deviation of the discrete model from the deterministic component. This scaling property can be proven at time zero with equilibrium initial data. Numerical simulations supports our conjecture that the scaling property remains to be true in later times. This explains theoretically the reason why dynamic hotspots have been observed associated with small criminal population in the discrete simulations of the SSRB model and the DTS Model [76]. And more, for general human behavior with similar aggregation pattern formation, our finding suggests that hotspot transience indicates a significant stochastic fluctuation in the martingale formulation, which could predict a small size of agents taking part in the activity.

There are two possible directions for the future work. On the one hand, we can assume independent Poisson clocks for each agent, which is more realistic to model typical criminal activities. Independent Poisson clocks will make the computations more complex though. It would be interesting to explore whether the *finite size effects* also occur. On the other hand, we can study parameterization of hotspot transience. This will give us a deeper understanding of the pattern formation in a complex system, e.g. pattern formation in fluid turbulence. This topic has been drawing a lot of interests recently ([31, 35, 38, 32]). But quantitative studies are lacking as far we know. The quantitative framework that we develop here could be applicable.

5 Appendix

To prove Theorem 2.1, we compute the infinitesimal means and variances of $\left\langle \left(B^{\ell}(t), n^{\ell}(t)\right), \phi^{\ell} \right\rangle$ for fixed ℓ ([1, 12, 16, 34, 36, 43, 47, 58, 59, 66, 68].

We first study related random variables. We assume that the Poisson-clock advances at t^-, and analyze the transition at time t. Conditioned on $(B^{\ell}(\mathbf{s},t^-), n^{\ell}(\mathbf{s},t^-))$, we observe that $E^{\ell}_{\mathbf{s}}(t)$, $\mathbf{s} \in \mathscr{S}$, is a family of independently identically distributed

Binomial random variables with the parameters $n^\ell(\mathbf{s},t^-)$ and $p^\ell(\mathbf{s},t^-)$, that is

$$\mathbb{P}\left(E_{\mathbf{s}}^\ell(t)=i\middle|B_{\mathbf{s}}^\ell(t^-),n_{\mathbf{s}}^\ell(t^-)\right)=\binom{n_{\mathbf{s}}^\ell(t^-)}{i}\left(p_{\mathbf{s}}^\ell(t^-)\right)^i(1-p_{\mathbf{s}}^\ell(t^-))^{n_{\mathbf{s}}^\ell(t^-)-i}, \quad (42)$$

where $i=0,1,2,...,n_{\mathbf{s}}^\ell(t^-)$. Hence we have

$$\mathbb{E}\left[E_{\mathbf{s}}^\ell(t)\middle|B_{\mathbf{s}}^\ell(t^-),n_{\mathbf{s}}^\ell(t^-)\right]=p_{\mathbf{s}}^\ell(t^-)n_{\mathbf{s}}^\ell(t^-), \quad (43)$$

$$\mathrm{Var}\left(E_{\mathbf{s}}^\ell(t)\middle|\left(B_{\mathbf{s}}^\ell(t^-),n_{\mathbf{s}}^\ell(t^-)\right),\forall\mathbf{s}\in\mathscr{S}\right)=n_{\mathbf{s}}^\ell(t^-)p_{\mathbf{s}}^\ell(t^-)\left[1-p_{\mathbf{s}}^\ell(t^-)\right]. \quad (44)$$

Let $J_{\mathbf{s},j}^\ell(t),\ j=1,2,...,n_{\mathbf{s}}^\ell(t^-)$ be a family of independently distributed Bernoulli random variables assuming 1 with probability $1-p_{\mathbf{s}}^\ell(t^-)$. If the j-th agent at site $\mathbf{s}$ chooses not to burglarize, then $J_{\mathbf{s},j}^\ell(t)$ assumes 1. This implies that

$$\mathbb{E}\left[\left(J_{\mathbf{s},j}^\ell(t)\right)^2\middle|\left(B_{\mathbf{s}}^\ell(t^-),n_{\mathbf{s}}^\ell(t^-)\right)\right]=\mathbb{E}\left[J_{\mathbf{s},j}^\ell(t)\middle|\left(B_{\mathbf{s}}^\ell(t^-),n_{\mathbf{s}}^\ell(t^-)\right)\right]=1-p_{\mathbf{s}}^\ell(t^-). \quad (45)$$

We also note that by our construction $E_{\mathbf{s}}^\ell(t)=\sum_{j=1}^{j=n_{\mathbf{s}}^\ell(t^-)}\left(1-J_{\mathbf{s},j}^\ell(t)\right)$.

Let $\Phi_{\mathbf{s},j}^\ell(t),\ j=1,...,n_{\mathbf{s}}^\ell(t^-)$ be a family of independently identically distributed random variables assuming $\phi_{\mathbf{s}'}$ with probability $A_{\mathbf{s}'}^\ell/T_{\mathbf{s}}^\ell$, for every $\mathbf{s}',\mathbf{s}'\sim\mathbf{s}$. Then we have

$$\mathbb{E}\left[\Phi_{\mathbf{s},j}^\ell(t)\middle|\left(B_{\mathbf{s}}^\ell(t^-),n_{\mathbf{s}}^\ell(t^-)\right),\forall\mathbf{s}\in\mathscr{S}^\ell\right]=\sum_{\substack{\mathbf{s}'\\ \mathbf{s}'\sim\mathbf{s}}}\phi_{\mathbf{s}'}^\ell\frac{A_{\mathbf{s}'}^\ell(t^-)}{T_{\mathbf{s}}^\ell(t^-)}, \quad (46)$$

$$\mathbb{E}\left[\left(\Phi_{\mathbf{s},j}^\ell(t)\right)^2\middle|\left(B_{\mathbf{s}}^\ell(t^-),n_{\mathbf{s}}^\ell(t^-)\right),\forall\mathbf{s}\in\mathscr{S}^\ell\right]=\sum_{\substack{\mathbf{s}'\\ \mathbf{s}'\sim\mathbf{s}}}\left(\phi_{\mathbf{s}'}^\ell\right)^2\frac{A_{\mathbf{s}'}^\ell(t^-)}{T_{\mathbf{s}}^\ell(t^-)}. \quad (47)$$

Let the number of replaced criminals on site $\mathbf{s}$ at time t be $\xi_{\mathbf{s}}^\ell(t)$. Then $\xi_{\mathbf{s}}^\ell(t)$ is a family of Bernoulli random variables assuming 1 with probability $\Gamma\ell^2/D$. Hence we have

$$\mathbb{E}\left[\xi_{\mathbf{s}}^\ell(t)\middle|\left(B_{\mathbf{s}}^\ell(t^-),n_{\mathbf{s}}^\ell(t^-)\right)\right]=\frac{\Gamma\ell^2}{D}, \quad (48)$$

$$\mathrm{Var}\left(\left(\xi_{\mathbf{s}}^\ell(t)\right)^2\middle|\left(B_{\mathbf{s}}^\ell(t^-),n_{\mathbf{s}}^\ell(t^-)\right)\right)=\frac{\Gamma\ell^2}{D}(1-\frac{\Gamma\ell^2}{D}). \quad (49)$$

Because the decision to burglarize is (conditionally) independent from the decision to move for each of the burglars, $J_{\mathbf{s},j}^\ell(t)$ and $\Phi_{\mathbf{k},h}^\ell(t)$ are (conditionally) independent for any choices of $\mathbf{s}$, $\mathbf{k}$, j and h. This implies that

$$
\begin{aligned}
&\mathbb{E}\left[J^\ell_{\mathbf{s},j}(t)\Phi^\ell_{\mathbf{s},j}(t)\middle|\left(B^\ell_{\mathbf{s}}(t^-),n^\ell_{\mathbf{s}}(t^-)\right),\forall \mathbf{s}\in\mathscr{S}^\ell\right]\\
&=\mathbb{E}\left[J^\ell_{\mathbf{s},j}(t)\middle|\left(B^\ell_{\mathbf{s}}(t^-),n^\ell_{\mathbf{s}}(t^-)\right),\forall \mathbf{s}\in\mathscr{S}^\ell\right]\mathbb{E}\left[\Phi^\ell_{\mathbf{s},j}(t)\middle|\left(B^\ell_{\mathbf{s}}(t^-),n^\ell_{\mathbf{s}}(t^-)\right),\forall \mathbf{s}\in\mathscr{S}^\ell\right]\\
&=\text{(by (45) and (46))}\\
&=\left[1-p^\ell_{\mathbf{s}}(t^-)\right]\sum_{\substack{\mathbf{s}'\\ \mathbf{s}'\sim\mathbf{s}}}\phi^\ell_{\mathbf{s}'}\frac{A^\ell_{\mathbf{s}'}(t^-)}{T^\ell_{\mathbf{s}}(t^-)},
\end{aligned}
\tag{50}
$$

$$
\begin{aligned}
&\mathrm{Var}\left(J^\ell_{\mathbf{s},j}(t)\Phi^\ell_{\mathbf{s},j}(t)\middle|\left(B^\ell_{\mathbf{s}}(t^-),n^\ell_{\mathbf{s}}(t^-)\right),\forall \mathbf{s}\in\mathscr{S}^\ell\right)\\
&=\mathbb{E}\left[\left(J^\ell_{\mathbf{s},j}(t)\Phi^\ell_{\mathbf{s},j}(t)\right)^2\middle|\left(B^\ell_{\mathbf{s}}(t^-),n^\ell_{\mathbf{s}}(t^-)\right),\forall \mathbf{s}\in\mathscr{S}^\ell\right]\\
&\quad-\left[\mathbb{E}\left[J^\ell_{\mathbf{s},j}(t)\Phi^\ell_{\mathbf{s},j}(t)\middle|\left(B^\ell_{\mathbf{s}}(t^-),n^\ell_{\mathbf{s}}(t^-)\right),\forall \mathbf{s}\in\mathscr{S}^\ell\right]\right]^2\\
&=\text{(by (45), (46), (47), and (45))}\\
&=\left[1-p^\ell_{\mathbf{s}}(t^-)\right]\sum_{\substack{\mathbf{s}'\\ \mathbf{s}'\sim\mathbf{s}}}\left(\phi^\ell_{\mathbf{s}'}\right)^2\frac{A^\ell_{\mathbf{s}'}(t^-)}{T^\ell_{\mathbf{s}}(t^-)}-\left[1-p^\ell_{\mathbf{s}}(t^-)\right]^2\left[\sum_{\substack{\mathbf{s}'\\ \mathbf{s}'\sim\mathbf{s}}}\phi^\ell_{\mathbf{s}'}\frac{A^\ell_{\mathbf{s}'}(t^-)}{T^\ell_{\mathbf{s}}(t^-)}\right]^2,
\end{aligned}
\tag{51}
$$

Right after the Poisson clock advances we have the following transition:

$$
\sum_{\mathbf{s}\in\mathscr{S}^\ell}n^\ell_{\mathbf{s}}(t)\phi^\ell_{\mathbf{s}}=\sum_{\mathbf{s}\in\mathscr{S}^\ell}\sum_{j=1}^{n^\ell_{\mathbf{s}}(t^-)}\left[1-J^\ell_{\mathbf{s},j}(t)\right]\Phi^\ell_{\mathbf{s},j}(t)+\sum_{\mathbf{s}\in\mathscr{S}^\ell}\xi^\ell_{\mathbf{s}}(t)\phi^\ell_{\mathbf{s}}.
\tag{52}
$$

With the above random variables we compute the infinitesimal means and variances. In the computational steps we will drop the super script ℓ for simplicity.

We compute the infinitesimal mean for $\left\langle B^\ell(t^-),\phi^\ell\right\rangle$. From (6) we have

$$
\begin{aligned}
&\mathscr{G}_1\left(\left\langle B^\ell(t^-),\phi^\ell\right\rangle,\left\langle n^\ell(t^-),\phi^\ell\right\rangle\right)\\
&=\frac{D}{\ell^2}\mathbb{E}\left[\ell^2\sum_{\mathbf{s}\in\mathscr{S}}\left[B_{\mathbf{s}}(t)-B_{\mathbf{s}}(t^-)\right]\phi_{\mathbf{s}}\middle|(B(t^-),n(t^-))\right]\\
&=\text{by (43)}\\
&=D\sum_{\mathbf{s}\in\mathscr{S}}\left[\left(1-\frac{\omega\ell^2}{D}\right)\frac{\eta\ell^2}{4}\Delta B_{\mathbf{s}}(t^-)-\frac{\omega\ell^2}{D}B_{\mathbf{s}}(t^-)+\theta p_{\mathbf{s}}(t^-)n_{\mathbf{s}}(t^-)\right]\phi_{\mathbf{s}},
\end{aligned}
\tag{53}
$$

which implies (11).

We compute the infinitesimal variance of $\left\langle B^\ell(t^-),\phi^\ell\right\rangle$:

$$
\begin{aligned}
&\mathscr{V}_1^\ell\left(\left\langle\left(B^\ell(t),n^\ell(t)\right),\phi^\ell\right\rangle\right)\\
&=\lim_{\delta t\to 0}\frac{1}{\delta t}\mathbb{E}\left[\left(\left\langle B(\delta t+t^-),\phi\right\rangle-\left\langle B(t^-),\phi\right\rangle\right)^2\middle|(B(t^-),n(t^-))\right]\\
&=\frac{D}{\ell^2}\mathbb{E}\left[\ell^4\left(\sum_{\mathbf{s}\in\mathscr{S}}B_{\mathbf{s}}(t^-)\phi_{\mathbf{s}}-\sum_{\mathbf{s}\in\mathscr{S}}B_{\mathbf{s}}(t)\phi_{\mathbf{s}}\right)^2\middle|\left(B(t^-),n(t^-)\right)\right]\\
&=D\ell^2\mathbb{E}\left[\sum_{\mathbf{s}\in\mathscr{S}}B_{\mathbf{s}}(t^-)\phi_{\mathbf{s}}-\sum_{\mathbf{s}\in\mathscr{S}}B_{\mathbf{s}}(t)\phi_{\mathbf{s}}\middle|\left(B(t^-),n(t^-)\right)\right]^2\\
&\qquad+D\ell^2\mathrm{Var}\left[\sum_{\mathbf{s}\in\mathscr{S}}B_{\mathbf{s}}(t^-)\phi_{\mathbf{s}}-\sum_{\mathbf{s}\in\mathscr{S}}B_{\mathbf{s}}(t)\phi_{\mathbf{s}}\middle|\left(B(t^-),n(t^-)\right)\right]\\
&:=J_1+J_2.
\end{aligned}
\tag{54}
$$

For J_1, from (53) we have

$$
J_1=\frac{\ell^2}{D}\mathscr{G}_1^2\left(\left\langle B(t^-),\phi\right\rangle,\left\langle n(t^-),\phi\right\rangle\right).
\tag{55}
$$

Then for J_2, we apply the independence of $E_{\mathbf{s}}(t)$ for distinct $\mathbf{s}\in\mathscr{S}$ and with (44) we obtain

$$
\begin{aligned}
J_2&=D\ell^2\mathrm{Var}\left(\sum_{\mathbf{s}\in\mathscr{S}}\left[\left(1-\frac{\omega\ell^2}{D}\right)\frac{\eta\ell^2}{4}\Delta B_{\mathbf{s}}(t^-)-\frac{\omega\ell^2}{D}B_{\mathbf{s}}(t^-)+\theta E_{\mathbf{s}}(t)\right]\phi_{\mathbf{s}}\middle|(B(t^-),n(t^-))\right)\\
&=D\ell^2\mathrm{Var}\left(\sum_{\mathbf{s}\in\mathscr{S}}\theta\phi_{\mathbf{s}}E_{\mathbf{s}}(t)\middle|(B(t^-),n(t^-))\right)\\
&=D\ell^2\sum_{\mathbf{s}\in\mathscr{S}}\theta^2\phi_{\mathbf{s}}^2\mathrm{Var}\left(E_{\mathbf{s}}(t)\middle|(B(t^-),n(t^-))\right)\\
&=D\ell^2\sum_{\mathbf{s}\in\mathscr{S}}\theta^2\phi_{\mathbf{s}}^2n_{\mathbf{s}}(t^-)p_{\mathbf{s}}(t^-)\left[1-p_{\mathbf{s}}(t^-)\right].
\end{aligned}
\tag{56}
$$

This together with (55) and (54) implies (13).

We compute the infinitesimal mean for $\left\langle n^\ell(t^-),\phi^\ell\right\rangle$. From (52) we have

$$
\begin{aligned}
&\mathscr{G}_2\left(\left\langle\left(B^\ell(t^-),n^\ell(t^-)\right),\phi^\ell\right\rangle\right)\\
&=\frac{D}{\ell^2}\mathbb{E}\left[\ell^2\sum_{\mathbf{s}\in\mathscr{S}}n_{\mathbf{s}}(t)\phi_{\mathbf{s}}-\ell^2\sum_{\mathbf{s}\in\mathscr{S}}n_{\mathbf{s}}(t)\phi_{\mathbf{s}}\middle|(B(t^-),n(t^-))\right]\\
&=D\sum_{\mathbf{s}\in\mathscr{S}}\mathbb{E}\left[\sum_{j=1}^{n_{\mathbf{s}}(t^-)}\left[1-J_{\mathbf{s},j}(t)\right]\Phi_{\mathbf{s},j}(t)+\xi_{\mathbf{s}}(t)\phi_{\mathbf{s}}-n_{\mathbf{s}}(t^-)\phi_{\mathbf{s}}\middle|(B(t^-),n(t^-))\right].
\end{aligned}
\tag{57}
$$

This together with (45), (46) and (48) implies

$$
\begin{aligned}
&\mathscr{G}_2\left(\left\langle\left(B^\ell(t^-),n^\ell(t^-)\right),\phi^\ell\right\rangle\right)\\
&=D\sum_{\mathbf{s}\in\mathscr{S}}\left[n_{\mathbf{s}}(t^-)\left[1-p_{\mathbf{s}}(t)\right]\sum_{\substack{\mathbf{s}'\\ \mathbf{s}'\sim\mathbf{s}}}\phi_{\mathbf{s}'}\frac{A_{\mathbf{s}'}(t^-)}{T_{\mathbf{s}}(t^-)}+\frac{\Gamma\ell^2}{D}\phi_{\mathbf{s}}-n_{\mathbf{s}}(t^-)\phi_{\mathbf{s}}\right]\\
&=D\sum_{\mathbf{s}\in\mathscr{S}}\left[\phi_{\mathbf{s}}A_{\mathbf{s}}(t^-)\sum_{\substack{\mathbf{s}'\\ \mathbf{s}'\sim\mathbf{s}}}\frac{n_{\mathbf{s}'}(t^-)\left[1-p_{\mathbf{s}'}(t)\right]}{T_{\mathbf{s}'}(t^-)}+\frac{\Gamma\ell^2}{D}\phi_{\mathbf{s}}-n_{\mathbf{s}}(t^-)\phi_{\mathbf{s}}\right],
\end{aligned}
\tag{58}
$$

which implies (12).

We compute the infinitesimal variance of $\left\langle n^\ell(t^-),\phi^\ell\right\rangle$

$$
\begin{aligned}
&\mathscr{V}_2^\ell\left(\left\langle\left(B^\ell(t),n^\ell(t)\right),\phi^\ell\right\rangle\right)\\
&=\lim_{\delta t\to 0}\frac{1}{\delta t}\mathbb{E}\left[\left(\left\langle n(\delta t+t^-),\phi\right\rangle-\left\langle n(t^-),\phi\right\rangle\right)^2\middle|\left(B(t^-),n(t^-)\right)\right]\\
&=D\ell^2\mathbb{E}\left[\sum_{\mathbf{s}\in\mathscr{S}}n_{\mathbf{s}}(t^-)\phi_{\mathbf{s}}-\sum_{\mathbf{s}\in\mathscr{S}}n_{\mathbf{s}}(t)\phi_{\mathbf{s}}\middle|\left(B(t^-),n(t^-)\right)\right]^2\\
&\qquad+D\ell^2\mathrm{Var}\left(\sum_{\mathbf{s}\in\mathscr{S}}n_{\mathbf{s}}(t^-)\phi_{\mathbf{s}}-\sum_{\mathbf{s}\in\mathscr{S}}n_{\mathbf{s}}(t)\phi_{\mathbf{s}}\middle|\left(B(t^-),n(t^-)\right)\right)\\
&:=J_3+J_4.
\end{aligned}
\tag{59}
$$

For J_3 we have

$$
J_3=\frac{\ell^2}{D}\mathscr{G}_2^2\left(\left\langle B(t^-),\phi\right\rangle,\left\langle n(t^-),\phi\right\rangle\right).
\tag{60}
$$

For J_4, with the independence of the related random variables, we obtain

$$
\begin{aligned}
J_4&=D\ell^2\sum_{\mathbf{s}\in\mathscr{S}}\mathrm{Var}\left(\sum_{j=1}^{n_{\mathbf{s}}(t^-)}J_{\mathbf{s},j}\Phi_{\mathbf{s},j}(t)+\xi_{\mathbf{s}}(t)\phi_{\mathbf{s}}-n_{\mathbf{s}}(t^-)\phi_{\mathbf{s}}\middle|\left(B(t^-),n(t^-)\right)\right)\\
&=D\ell^2\sum_{\mathbf{s}\in\mathscr{S}}\mathrm{Var}\left(\xi_{\mathbf{s}}(t)\phi_{\mathbf{s}}\middle|\left(B(t^-),n(t^-)\right)\right)\\
&\quad+D\ell^2\sum_{\mathbf{s}\in\mathscr{S}}n_{\mathbf{s}}(t^-)\mathrm{Var}\left(J_{\mathbf{s},j}(t)\Phi_{\mathbf{s},j}(t)\middle|\left(B(t^-),n(t^-)\right)\right)\\
&:=J_{4,1}+J_{4,2}.
\end{aligned}
\tag{61}
$$

For $J_{4,1}$, by (49) we have

$$
J_{4,1}=\ell^4\Gamma\left(1-\frac{\Gamma\ell^2}{D}\right)\sum_{\mathbf{s}\in\mathscr{S}}\phi_{\mathbf{s}}^2.
\tag{62}
$$

For $J_{4,2}$, by (50) and (51) we have

$$J_{4,2} = D\ell^2 \sum_{\mathbf{s}\in\mathscr{S}} n_{\mathbf{s}}(t^-) p_{\mathbf{s}}(t^-)\left[1-p_{\mathbf{s}}(t^-)\right]\left[\sum_{\substack{\mathbf{s}'\\ \mathbf{s}'\sim\mathbf{s}}} \phi_{\mathbf{s}'}\frac{A_{\mathbf{s}'}(t^-)}{T_{\mathbf{s}}(t^-)}\right]^2$$
$$+ D\ell^2 \sum_{\mathbf{s}\in\mathscr{S}} n_{\mathbf{s}}(t^-)\left[1-p_{\mathbf{s}}(t^-)\right]\left[\sum_{\substack{\mathbf{s}'\\ \mathbf{s}'\sim\mathbf{s}}} \phi_{\mathbf{s}'}^2\frac{A_{\mathbf{s}'}(t^-)}{T_{\mathbf{s}}(t^-)} - \left(\sum_{\substack{\mathbf{s}'\\ \mathbf{s}'\sim\mathbf{s}}} \phi_{\mathbf{s}'}\frac{A_{\mathbf{s}'}(t^-)}{T_{\mathbf{s}}(t^-)}\right)^2\right]$$
$$:= J_{4,1,1} + J_{4,1,2}. \tag{63}$$

We simplify $J_{4,1,2}$ as follows

$$J_{4,1,2} = D\ell^2 \sum_{\mathbf{s}\in\mathscr{S}} n_{\mathbf{s}}(t^-)\left[1-p_{\mathbf{s}}(t^-))\right]\sum_{\substack{\mathbf{s}'\\ \mathbf{s}'\sim\mathbf{s}}}\frac{A_{\mathbf{s}'}(t^-)}{T_{\mathbf{s}}(t^-)}\left[\phi_{\mathbf{s}'} - \sum_{\substack{\mathbf{s}'\\ \mathbf{s}'\sim\mathbf{s}}}\phi_{\mathbf{s}'}\frac{A_{\mathbf{s}'}(t^-)}{T_{\mathbf{s}}(t^-)}\right]^2$$
$$= D\ell^2 \sum_{\mathbf{s}\in\mathscr{S}} n_{\mathbf{s}}(t^-)\left[1-p_{\mathbf{s}}(t^-)\right]\sum_{\substack{\mathbf{s}'\\ \mathbf{s}'\sim\mathbf{s}}}\frac{A_{\mathbf{s}'}(t^-)}{T_{\mathbf{s}}(t^-)}\left[\sum_{\substack{\mathbf{s}''\\ \mathbf{s}''\neq\mathbf{s}'\\ \mathbf{s}''\sim\mathbf{s}}}(\phi_{\mathbf{s}'}-\phi_{\mathbf{s}''})\frac{A_{\mathbf{s}''}(t^-)}{T_{\mathbf{s}}(t^-)}\right]^2. \tag{64}$$

This together with (59)-(63) implies (14).

With the infinitesimal means and variances we apply Theorem (1.6), [14] or Theorem 3.32, [51], to arrive at (9), and apply Exercise 3.8.12 of [6], Lemma A 1.5.1, [44], or Proposition B.1 in [64][3] to obtain (10). To conclude the proof of Theorem 2.1 is completed.

Acknowledgments

We would like to thank the helpful discussions with Prof. A. Debussche, Prof. Andrea Montanari, Prof. Thomas Liggett, Prof. Carl Mueller, Prof. Wotao Yin, Mac Jugal Nankep Nguepedja, Da Kuang, Yifan Chen, Fangbo Zhang, Yu Gu, Jingyu Huang, Yatin Chow, Wuchen Li and Kenneth Van. A. Bertozzi is supported by NSF grant DMS-1737770 and M. Short is supported by NSF grant DMS-1737925.

[3] In [64], one can directly compute Γ_f and obtain that when $f = Id$ then the infinitesimal variance comes up.

References

1. D. Applebaum, **Lévy processes and stochastic calculus**, Cambridge University Press, Cambridge, (2009).
2. G. J. Babu and E. D. Feigelson, Spatial point processes in astronomy, *J. Statist. Plann. Inference*, **50**, 311–326, (2015).
3. N. Bellomo, F. Colasuonno, D. Knopoff, and J. Soler, From a systems theory of sociology to modeling the onset and evolution of criminality, *Netw. Het. Media*, **10**, 421–441, (2015).
4. H. Berestycki, N. Rodríguez, and L. Ryzhik, Traveling wave solutions in a reaction-diffusion model for criminal activity, *Multiscale Model. Simul.*, **11**, 1097–1126, (2013).
5. M. Bertero, P. Boccacci, G. Desiderà, and G. Vicidomini, Image deblurring with Poisson data: from cells to galaxies, *Inverse Problems*, **25**, paper n. 123006, 26 (2009).
6. K. Bichteler, **Stochastic integration with jumps**, Cambridge University Press, Cambridge, (2002).
7. D. Brockmann, L. Hufnagel, and T. Geisel, The scaling laws of human travel, *Nature*, **439**, 462–465, (2006).
8. T. Budd, *Burglary of domestic dwellings: Findings from the British Crime Survey,* Home Office Statistical Bulletin, Vol. 4 (Government Statistical Service, London, 1999).
9. L. Cao and M. Grabchak, Smoothly truncated levy walks: Toward a realistic mobility model, *2014 IEEE 33rd Int. Performance Computing and Communications Conference, (IPCCC)*, 5–7 December 2014, Austin, Texas, USA, pp. 1–8.
10. S. Chaturapruek, J. Breslau, D. Yazdi, T. Kolokolnikov, and S. G. McCalla, Crime modeling with Lévy flights, *SIAM J. Appl. Math.*, **73**, 1703–1720, (2013).
11. S. N. Chow, W. Li, and H. Zhou, Entropy dissipation of Fokker-Planck equations on graphs, *Discrete Contin. Dyn. Syst.*, **38**, 4929–4950, (2018).
12. K. L. Chung and R. J. Williams, **Introduction to stochastic integration**, Birkhäuser/Springer, New York, (2014).
13. L. Citi, D. Ba, E. N. Brown, and R. Barbieri, Likelihood methods for point processes with refractoriness, *Neural Comput.*, **26**, 237–263, (2014).
14. R. Durrett, **Stochastic calculus**, CRC Press, Boca Raton, FL, (1996).
15. R. Durrett, **Essentials of stochastic processes**, Springer-Verlag, New York, (1999).
16. R. Durrett, **Probability models for DNA sequence evolution**, Springer-Verlag, New York, (2002).
17. R. Durrett, **Probability: theory and examples**, Cambridge University Press, Cambridge, (2010).
18. P. Embrechts, R. Frey, and H. Furrer, Stochastic processes in insurance and finance, in **Stochastic processes: theory and methods**. North-Holland, Amsterdam, 365–412, (2001).
19. S. N. Ethier and T. G. Kurtz, **Markov processes**, John Wiley & Sons, Inc., New York, (1986).
20. M. Erbar and J. Maas, Ricci curvature of finite Markov chains via convexity of the entropy, *Arch. Ration. Mech. Anal*, **206**, 997–1038, (2012) .
21. M. Erbar and J. Maas, Gradient flow structures for discrete porous medium equations, *Discrete Contin. Dyn. Syst.*, **34**, 1355–1374, (2014).
22. M. Fathi and J. Maas, Entropic Ricci curvature bounds for discrete interacting systems, *Ann. Appl. Probab.*, **26**, 1774–1806, (2016).
23. G. Farrell and K. Pease, **Repeat Victimization**, Criminal Justice Press, (2001).
24. T. Franco, Interacting particle systems: hydrodynamic limit versus high density limit, in **From particle systems to partial differential equations**. Springer, Heidelberg, 179–189, (2014).
25. J. M. Gau and T. C. Pratt, Revisiting broken windows theory: Examining the sources of the discriminant validity of perceived disorder and crime, *J. Crim. Justice*, **38**, 758–766, (2010).
26. M. C. Gonzlez, C. A. Hidalgo, and A.-L. Barabsi, Understanding individual human mobility patterns, *Nature*, **453**, 779–782, (2008).
27. I. J. Good, Some statistical applications of Poisson's work, *Statist. Sci.*, **1**, 157–180, (1986).
28. W. Gorr and Y. Lee, Early warning system for temporary crime hot spots, *J. Quant. Criminol.*, **31**, 25–47, (2015).

29. T. Goudon, B. Nkonga, M. Rascle, and M. Ribot, Self-organized populations interacting under pursuit-evasion dynamics, *Phys. D*, **304/305**, 1–22, (2015).
30. M. Z. Guo, G. C. Papanicolaou, and S. R. S. Varadhan, Nonlinear diffusion limit for a system with nearest neighbor interactions, *Comm. Math. Phys.*, **118**, 31–59, (1988).
31. F. Hamba, Turbulent energy density in scale space for inhomogeneous turbulence, *J. Fluid Mech.*, **842**, 532–553, (2018).
32. I. Hameduddin, C. Meneveau, T A. Zaki, and D. F. Gayme, Geometric decomposition of the conformation tensor in viscoelastic turbulence, *J. Fluid Mech.*, **842**, 395–427, (2018).
33. B. E. Harcourt, Reflecting on the subject: A critique of the social influence conception of deterrence, the broken windows theory, and order-maintenance policing New York style, *Michigan Law Rev.*, **97**, 291–389, (1998).
34. S. W. He, J. G. Wang, and J. A. Yan, **Semimartingale theory and stochastic calculus**, Kexue Chubanshe (Science Press), Beijing; CRC Press, Boca Raton, FL, (1992).
35. S. J. Illingworth, J. P. Monty, and I. Marusic, Estimating large-scale structures in wall turbulence using linear models, *J. Fluid Mech.*, **842**, 146–162, (2018).
36. J. Jacod and A. N. Shiryaev, **Limit theorems for stochastic processes**, Springer-Verlag, Berlin, (2003).
37. A. James, M. J. Plank, and A. M. Edwards, Assessing Lévy walks as models of animal foraging, *J. R. Soc. Interface*, **8**, 1233–1247, (2011).
38. J. Jiménez, Coherent structures in wall-bounded turbulence, *J. Fluid Mech.*, **842**, P1, 100, (2018).
39. S. D. Johnson, W. Bernasco, K. J. Bowers, H. Elffers, J. Ratcliffe, G. Rengert, and M. Townsley, Space-time patterns of risk: A cross national assessment of residential burglary victimization, *J. Quant. Criminol.*, **23**, 201–219, (2007).
40. S. D. Johnson and K. J. Bowers, The stability of space-time clusters of burglary, *Br. J. Criminol.*, **44**, 55–65, (2004).
41. S. D. Johnson, K. Bowers, and A. Hirschfield, New insights into the spatial and temporal distribution of repeat victimization, *Br. J. Criminol.*, **37**, 224–241, (1997).
42. P. A. Jones, P. J. Brantingham, and L. R. Chayes, Statistical models of criminal behavior: the effects of law enforcement actions, *Math. Models Methods Appl. Sci.*, **20**, 1397–1423, (2010).
43. S. Karlin and H. M. Taylor, **A second course in stochastic processes**, Academic Press, Inc. [Harcourt Brace Jovanovich, Publishers], New York-London, (1981).
44. C. Kipnis, and C. Landim, **Scaling limits of interacting particle systems**, Springer-Verlag, Berlin, (1999).
45. C. Kipnis, S. Olla, and S. R. S. Varadhan, Hydrodynamics and large deviation for simple exclusion processes, *Comm. Pure Appl. Math.*, **42**, 115–137, (1989).
46. T. Kolokolnikov, M. J. Ward and J. Wei, The stability of steady-state hot-spot patterns for a reaction-diffusion model of urban crime, *Discrete Contin. Dyn. Syst. Ser. B*, **19**, 1373–1410, (2014).
47. T. M. Liggett, **Lectures on stochastic flows and applications**, Published for the Tata Institute of Fundamental Research, Bombay; by Springer-Verlag, Berlin, (1986).
48. T. Levajković, H. Mena, and M. Zarfl, Lévy processes, subordinators and crime modeling, *Novi Sad J. Math.* **46**, 65–86, (2016).
49. T. M. Liggett, Interacting Markov processes, in **Biological growth and spread (Proc. Conf., Heidelberg, 1979)**. Springer, Berlin-New York, 145–156, (1980).
50. T. M. Liggett, **Interacting particle systems**, Springer-Verlag, New York, (1985).
51. T. M. Liggett, **Continuous time Markov processes**, American Mathematical Society, Providence, RI, (2010).
52. D. J. B. Lloyd and H. O'Farrell, On localised hotspots of an urban crime model, *Phys. D*, **253**, 23–39, (2013).
53. R. N. Mantegna and H. E. Stanley, Stochastic process with ultraslow convergence to a Gaussian: the truncated Lévy flight, *Phys. Rev. Lett.*, **73**, 2946–2949, (1994).
54. M. C. Mariani and Y. Liu, Normalized truncated Levy walks applied to the study of financial indices, *Physica A, Stat. Mech. Appl.*, **377**, 590–598, (2007).

55. G. Ajmone Marsan, N. Bellomo, and L. Gibelli, Stochastic evolutionary differential games toward a systems theory of behavioral social dynamics, *Math. Models Methods Appl. Sci.*, **26**, 1051–1093, (2016).
56. A. Matacz, Financial modeling and option theory with the truncated Lévy process, *Int. J. Theor. Appl. Financ.*, **3**, 143–160, (2000).
57. S. G. McCalla, M. B. Short, and P. J. Brantingham, The effects of sacred value networks within an evolutionary, adversarial game, *J. Stat. Phys.*, **151**, 673–688, (2013).
58. M. Métivier, **Semimartingales**, Walter de Gruyter & Co., Berlin-New York, (1982).
59. M. Métivier and J. Pellaumail, **Stochastic integration**, Academic Press [Harcourt Brace Jovanovich, Publishers], New York-London-Toronto, Ont., (1980).
60. L. C. Miranda and R. Riera, Truncated Lévy walks and an emerging market economic index, *Physica A, Stat. Mech. Appl.*, **297**, 509–520, (2001) .
61. G. O. Mohler, M. B. Short, and P. J. Brantingham, The concentration-dynamics tradeoff in crime hot spotting, in **Unraveling the Crime-Place Connection** Vol. 22 (Routledge, 2017), pp. 19-40.
62. G. O. Mohler, M. B. Short, P. J. Brantingham, F. P. Schoenberg, and G. E. Tita, Self-exciting point process modeling of crime, *J. Am. Stat. Assoc.*, **106**, 100–108, (2011) .
63. G. O. Mohler, M. B. Short, S. Malinowski, M. Johnson, G. E. Tita, A. L. Bertozzi, and P. J. Brantingham, Randomized controlled field trials of predictive policing, *J. Am. Stat. Assoc.*, **110**, 1399–1411, (2015) .
64. J. Mourrat, A quantitative central limit theorem for the random walk among random conductance, *Electron. J. Probab.*, **17**, no. 97, 17, (2012).
65. H. G. Othmer, S. R. Dunbar, and W. Alt, Models of dispersal in biological systems, *J. Math. Biol.*, **26**, 263–298, (1988).
66. S. Peszat and J. Zabczyk, **Stochastic partial differential equations with Lévy noise**, Cambridge University Press, Cambridge, (2007).
67. A. B. Pitcher, Adding police to a mathematical model of burglary, *European J. Appl. Math.*, **21**, 401–419, (2010).
68. P. E. Protter, **Stochastic integration and differential equations**, Springer-Verlag, Berlin, (2005).
69. S. R. S. Varadhan, Entropy methods in hydrodynamic scaling, in **Proceedings of the International Congress of Mathematicians, Vol. 1, 2 (Zürich, 1994)**. Birkhäuser, Basel, 196–208, (1995).
70. S. R. S. Varadhan, Lectures on hydrodynamic scaling, in **Hydrodynamic limits and related topics (Toronto, ON, 1998)**. Amer. Math. Soc., Providence, RI, 3–40, (2000).
71. N. Rodríguez, On the global well-posedness theory for a class of PDE models for criminal activity, *Phys. D*, **260**, 191–200, (2013) .
72. N. Rodríguez and A. L. Bertozzi, Local existence and uniqueness of solutions to a PDE model for criminal behavior, *Math. Models Methods Appl. Sci.*, **20**, 1425–1457, (2010).
73. M. B. Short, A. L. Bertozzi, and P. J. Brantingham, Nonlinear patterns in urban crime: hotspots, bifurcations, and suppression, *SIAM J. Appl. Dyn. Syst.*, **9**, 462–483, (2010).
74. M. B. Short, P. J. Brantingham, A. L. Bertozzi, and G. E. Tita, Dissipation and displacement of hotspots in reaction-diffusion models of crime, *Proc. Natl. Acad. Sci.*, **107**, 3961–3965, (2010).
75. M. B. Short, M. R. D'Orsogna, P. J. Brantingham, and G. E. Tita, Measuring and modeling repeat and near-repeat burglary effects, *J. Quant. Criminol.*, **25**, 325–339, (2009).
76. M. B. Short, M. R. D'Orsogna, V. B. Pasour, G. E. Tita, P. J. Brantingham, A. L. Bertozzi, and L. B. Chayes, A statistical model of criminal behavior, *Math. Models Methods Appl. Sci.*, **18**, 1249–1267, (2008).
77. M. B. Short, G. O. Mohler, P. J. Brantingham, and G. E. Tita, Gang rivalry dynamics via coupled point process networks, *Discrete Contin. Dyn. Syst. Ser. B*, **19**, 1459–1477, (2014).
78. B. Snook, Individual differences in distance travelled by serial burglars, *J. Investig. Psych. Offender Profil.* **1**, 53–66, (2004).
79. D. W. Stroock and S. R. S. Varadhan, **Multidimensional diffusion processes**, Springer-Verlag, Berlin, (2006).

80. B. Tóth and B. Valkó, Onsager relations and Eulerian hydrodynamic limit for systems with several conservation laws, *J. Statist. Phys.*, **112**, 497–521, (2003).
81. W. H. Tse and M. J. Ward, Hotspot formation and dynamics for a continuum model of urban crime, *European J. Appl. Math.* **27**, 583–624, (2016).
82. P. J. van Koppen and R. W. J. Jansen, The road to the robbery: Travel patterns in commercial robberies, *Brit. J. Criminol.* **38**, 230–246, (1998).
83. J. Q. Wilson and G. L. Kelling, Broken windows: The police and neighborhood safety, *Atlantic Mon.* **249**, 29–38, (1982).
84. J. R. Zipkin, M. B. Short, and A. L. Bertozzi, Cops on the dots in a mathematical model of urban crime and police response, *Discrete Contin. Dyn. Syst. Ser. B* **19**, 1479–1506, (2014).